

Gene regulatory network structure informs the distribution of perturbation effects

Matthew Aguirre¹, Jeffrey P. Spence², Guy Sella^{3,4}, Jonathan K. Pritchard^{2,5}

¹ Department of Biomedical Data Science, Stanford University, Stanford CA

² Department of Genetics, Stanford University, Stanford CA

³ Department of Biological Sciences, Columbia University, New York NY

⁴ Program for Mathematical Genomics, Columbia University, New York NY

⁵ Department of Biology, Stanford University, Stanford CA

Correspondence to:

magu@stanford.edu, jspence@stanford.edu,
gs2747@columbia.edu, pritch@stanford.edu

July 4, 2024

Abstract

Gene regulatory networks (GRNs) govern many core developmental and biological processes underlying human complex traits. Even with broad-scale efforts to characterize the effects of molecular perturbations and interpret gene coexpression, it remains challenging to infer the architecture of gene regulation in a precise and efficient manner. Key properties of GRNs, like hierarchical structure, modular organization, and sparsity, provide both challenges and opportunities for this objective. Here, we seek to better understand properties of GRNs using a new approach to simulate their structure and model their function. We produce realistic network structures with a novel generating algorithm based on insights from small-world network theory, and we model gene expression regulation using stochastic differential equations formulated to accommodate modeling molecular perturbations. With these tools, we systematically describe the effects of gene knockouts within and across GRNs, finding a subset of networks that recapitulate features of a recent genome-scale perturbation study. With deeper analysis of these exemplar networks, we consider future avenues to map the architecture of gene expression regulation using data from cells in perturbed and unperturbed states, finding that while perturbation data are critical to discover specific regulatory interactions, data from unperturbed cells may be sufficient to reveal regulatory programs.

22 1 Introduction

23 In the past decade, single cell sequencing assays have been instrumental in enabling functional
24 studies of gene regulatory networks (GRNs). Observational studies of single cells have revealed
25 substantial diversity and heterogeneity in the cell types that comprise healthy and diseased tis-
26 sues [1], and molecular models of transcriptional systems have been used to understand the de-
27 velopmental processes involved in maintaining cell state and cell cycle [2, 3]. Meanwhile, recent
28 advances in the design of interventional studies, including CRISPR-based molecular perturbation
29 approaches like Perturb-seq [4,5], have been useful for learning the local structure of GRNs around
30 a focal gene or pathway [6, 7], discovering trait-relevant gene sets at scale [8], and determining
31 novel functions for poorly characterized genes in a particular cell type [9]. The preponderance of
32 single-cell data in multiple cell types, tissues, and contexts has also fueled a resurgence of interest
33 in the wholesale inference of GRNs, capitalizing on new techniques from graph theory and causal
34 inference [10,11].

35 In functional genomics, network inference and candidate gene prioritization are typical aims of
36 experimental data analysis. In this setting, it is common to make assumptions about the structure
37 and function of GRNs to enable convenient computation. In particular, linear models of gene
38 expression on directed acyclic graphs (DAGs) have been foundational for studies of GRNs, and
39 this approach to structure learning is well-described in the literature [12, 13]. Many extensions
40 based on this framework have been proposed, including additional sparsity constraints in the
41 form of regression penalties or low-rank assumptions [14, 15]. Analogous techniques have also
42 been used in the algorithmic design of perturbation experiments [16].

43 Even though convenience assumptions like linearity and acyclicity are rarely seen as limiting
44 in practice, it is important to note that they are not always biologically realistic. Gene regula-
45 tion is known to contain extensive feedback mechanisms [6], and some regulatory structures (in
46 particular, triangles, like the feed-forward motif [17, 18]) are not captured well by low-rank rep-
47 resentations of GRNs [19]. Furthermore, biological networks are thought to be well described
48 by directed graphs with hierarchical organization and with a degree-distribution that follows an
49 approximate power-law [20–22]. In network inference, it is less common to make explicit use of
50 these properties, though there are notable exceptions [7, 23].

51 With these practical considerations in mind, it is worth critically examining assumptions which
52 are (or could be) made about the structure of GRNs. In network theory, there are well-established
53 models of networks with group structure [24,25] and with scale-free topologies [26–28]. The defin-
54 ing feature of directed scale-free graphs is a power-law distribution of node in- and out-degrees:
55 this yields emergent properties including group-like structure and enrichment for structural mo-
56 tifs [18]. Further, most nodes in these graphs are connected to one another by short paths, which
57 is referred to as the “small-world” property of networks [29,30].

58 Here, we characterize in detail a set of structural properties that we consider to be highly
59 relevant for the study of GRNs. We propose a new algorithm to generate synthetic networks
60 with these properties and formulate a gene expression model to simulate data from them. We
61 use this simulation framework to conduct an array of *in silico* functional genomic studies and
62 characterize the parameter space of our model in light of a recent genome-wide Perturb-seq study
63 [9]. Our results provide intuition about the effects of various graph properties and how they
64 manifest in experimental data. We conclude by discussing implications for future efforts to map

65 the architecture of gene regulation and complex traits, with particular emphasis on identifying
66 pairwise regulatory relationships between genes and clustering genes into programs. Our analysis
67 tools are available on github as a resource to the scientific community.

68 2 Main

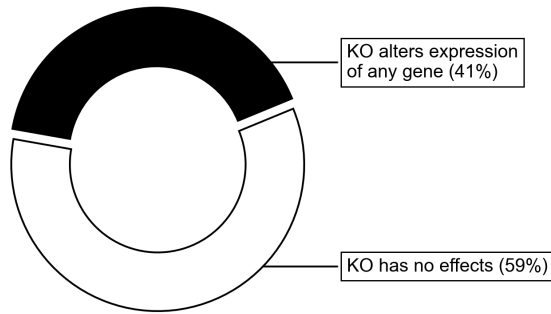
69 2.1 Modeling approach

70 Inspired by previous work from network theory and systems biology, we list what we consider
71 to be key properties of GRNs. We motivate these criteria in light of a recent genome-scale study
72 of genetic perturbations, conducted in an erythroid progenitor cell line (K562) (**Fig. 1**) [9]. To
73 date, this is one of the largest available single-cell and single-gene perturbation datasets in any
74 cell type: the data contain measurements on the expression of 5,530 gene transcripts in 1,989,578
75 cells, which were subject to 11,258 CRISPR-based perturbations of 9,866 unique genes. Here, we
76 subset these data to 5,247 perturbations that target genes whose expression is also measured in
77 the data (**Methods**). Key network properties are as follow:

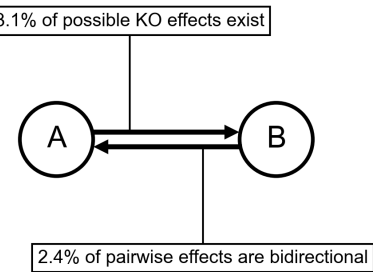
- 78 1. **GRNs are sparse:** While gene expression is controlled by many variables, the typical gene is
79 directly affected by a small number of regulators. We further expect the number of regulators
80 of any single gene to be much smaller than the total number of regulators in the network.
81 Also, not all genes participate in expression regulation: only 41% of perturbations that target
82 a primary transcript have significant effects on the expression of any other gene (**Fig. 1A**).
- 83 2. **GRNs have directed edges and feedback loops:** Regulatory relationships between genes
84 are directed, with one gene acting as a regulator and the other as a target gene: this means
85 that “A regulates B” is distinct from “B regulates A”. Meanwhile, feedback loops are also
86 thought to be pervasive in gene regulatory networks. A simple case of a feedback loop is
87 bidirectional regulation, which is observed in data: 3.1% of ordered gene pairs have at least
88 a one-directional perturbation effect (i.e., “A affects B”, Anderson-Darling FDR-corrected
89 $p < 0.05$), and 2.4% of these pairs further have bi-directional effects (i.e., “B also affects A”)
90 (**Fig. 1B**).
- 91 3. **GRNs have asymmetric distributions of in- and out-degree:** A further asymmetry between
92 regulators and target genes arises from the existence of master regulators, which directly par-
93 ticipate in the regulation of many other genes. The number of regulators per gene and genes
94 per regulator are both thought to follow an approximate power-law distribution [20, 21],
95 and indeed, the number of perturbation effects per regulator has a heavier-tailed distribu-
96 tion than the number of effects per target gene (**Fig. 1C**).
- 97 4. **GRNs are modular:** Genes in regulatory networks have different molecular functions that
98 are executed in concert across various cell and tissue types. This grouping of genes by func-
99 tion also corresponds to a hierarchical organization of regulatory relationships that is re-
100 vealed when these programs respond similarly to certain sets of perturbations (**Fig. 1D**).

101 While these criteria are not exhaustive, they do substantially constrain the space of plausible
102 GRN structures. But from first principles, it is not obvious how these properties of GRNs manifest

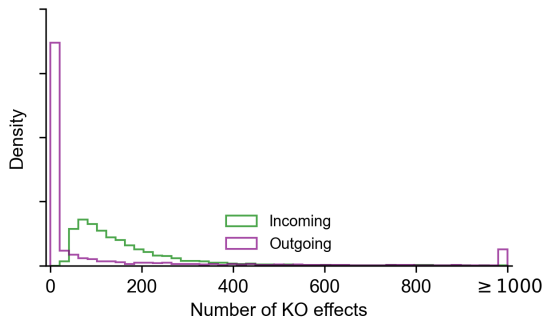
A: Perturbation effects are sparse



B: Edges are directed and can form loops



C: Degree distributions are asymmetric



D: Genes are organized into modules

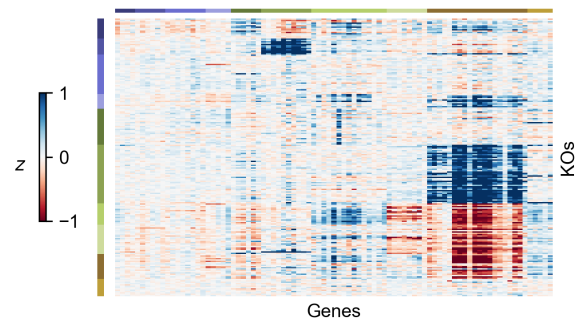


Figure 1: **Key properties of gene regulatory networks.** Data from Replogle *et. al.*, 2022. **(A)** Of the 5,247 perturbations in our analysis subset, 2,152 (41%) have a measurable effect on the transcriptional state of cells (energy-test $p < 0.001$). **(B)** Among all ordered pairs of genes, 3.1% (865,719 pairs) have a one-directional effect (FDR-corrected $p < 0.05$). Of these pairs with KO effects, 2.4% (20,621 pairs) further have bidirectional effects. **(C)** Summaries of the distribution of KO effects (Anderson-Darling $p < 0.05$) from the perspective of genes as subject to perturbation (outgoing effects) and as target genes when other genes are perturbed (incoming effects). **(D)** Subset of z -normalized expression data corresponding to 10 gene modules, using labels as provided in the dataset – each modules is labeled by a color in the to bars above the x - and y -axes, and z -scores are clipped at ± 1 , for visualization.

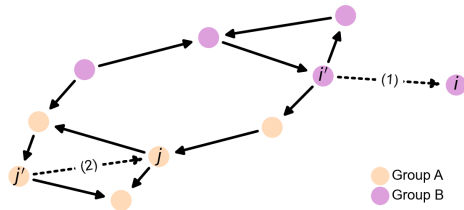
103 in an ever-growing body of experimental data. In other words, what does it matter that networks
104 are sparse, or modular?

105 2.2 Network generating algorithm

106 To better understand these foundational questions about the architecture of gene expression reg-
107 ulation, we propose a two-step process to simulate synthetic GRNs. First, we produce realistic
108 graph structures using a novel generating algorithm: we show that its parameters control key
109 properties of the resulting graphs. Second, we describe a dynamical systems model of gene ex-
110 pression, which we use to generate synthetic data from arbitrary graph structures. With these
111 tools, we conduct an array of simulated molecular perturbation studies, varying network proper-
112 ties of interest: an overview of our network generating algorithm is in Fig. 2A.

113 Our algorithm is based on that of Bollobas *et. al.*, 2003 [28], which models network growth

A: Overview of network generating algorithm



Parameters for 1,920 GRNs in this study:

- Number of genes (n): 2000
- Number of groups (k): 1, ..., 100
- Sparsity term (p): 1/2, ..., 1/16
- In-group term (w): 1, ..., 900
- In-degree term (δ_{in}): 10, ..., 300
- Out-degree term (δ_{out}): 1, ..., 30

Perform one of these two steps at random, until the graph has n nodes:

- (1). With prob. p : Attach a new node (i) with an incoming edge. Pick the source (i') using out-degrees (δ_{out}) and groups (w).
- (2). With prob. $1 - p$: Add a new edge. Pick the target (j) using in-degrees (δ_{in}), and the source (j') using out-degrees (δ_{out}) and groups (w).

B: Graph properties controlled by algorithm parameters

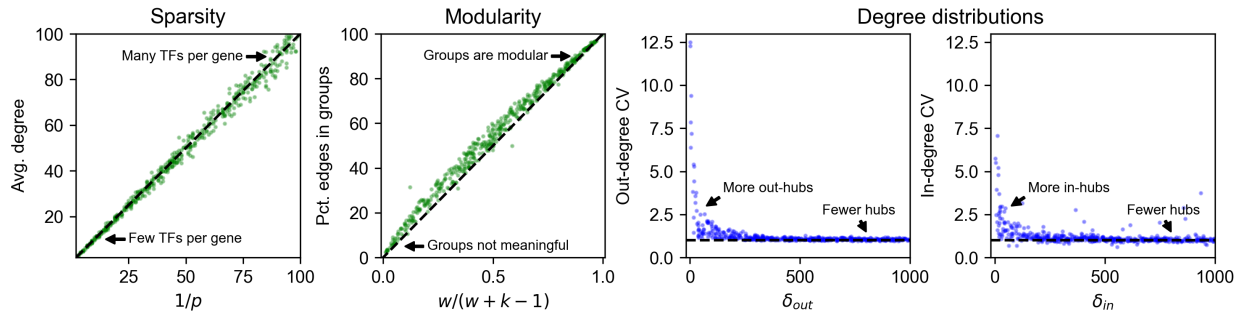


Figure 2: Modeling approach and network generating algorithm. (A) Overview of network generating algorithm, based on a growth process with preferential attachment. At each step, randomly add either a node or an edge, with the source and target determined by the out- and in-degree distributions, and node membership in groups. (B) Key graph properties can be tuned by changing the parameters of the generating algorithm. We validate this in 1,000 synthetic graphs with 500 nodes each, produced with various generating parameters. The same networks are plotted in all four panels, indicating robustness across different background distributions of parameters.

114 with preferential attachment. This algorithm starts with a small initial graph, and randomly adds
 115 nodes or directed edges until the graph reaches a pre-specified size. When adding a node, the new
 116 node is selected to be the target of a new directed edge. When adding an edge between existing
 117 nodes, a node is selected to be the target with a probability that increases with the number of
 118 outgoing edges it already has. When selecting a node to be the source of a new edge (i.e., to be
 119 the regulator for a new gene, if we are adding a node, or for an existing gene, if we are adding an
 120 edge), we select with probability increasing in the number of incoming edges it already has. Our
 121 work extends this algorithm in two ways: first, by assigning each node in the network to one of
 122 a number of pre-specified groups, and second, by specifying a within-group affinity term which
 123 biases edges to be drawn between members of the same group. The full procedure, including
 124 pseudocode and a description of its parameters, is given by **Algorithm 1**.

125 The output of our algorithm is a directed scale-free network on n nodes, each of which is
 126 assigned to one of k groups. The parameters in our algorithm control specific network properties.
 127 To show this, we generated 1,000 synthetic graphs with $n = 500$ genes using an array of randomly
 128 sampled parameters (**Fig. 2B**). We observe that the sparsity term p adjusts the mean number
 129 of regulators per gene, which is approximately $1/p$ (**Fig. 2B**). The number of groups k and the

Algorithm 1 Directed scale-free network with groups

Require:

- n : Number of genes (nodes) in the network ($n \geq 3$).
- k : Number of groups in the network ($1 \leq k \leq n$).
- p : Sparsity term ($0 < p \leq 1$).
- δ_{in} : In-degree biasing term ($\delta_{in} \geq 0$).
- δ_{out} : Out-degree biasing term ($\delta_{out} \geq 0$).
- w : Group biasing term ($w \geq 1$).

```

▷ Initialize the graph  $G$  to be a three-node cycle. Assign each node to its own group. ◁
 $G \leftarrow \{(1 \rightarrow 2), (2 \rightarrow 3), (3 \rightarrow 1)\}$ 
 $gp(i) \leftarrow i, \quad i \in \{1, 2, 3\}$  ◁ If  $k = 2$  then assign node 3 to group 1.

▷ Grow the graph  $G$  according to the below steps, until it has  $n$  genes. ◁
while  $|G| < n$  do
  ▷ Pick a gene (node)  $i$  to be the target of a new regulatory relationship (edge). With probability  $p$ ,
  add a new gene to  $G$ , otherwise pick an existing gene proportional to the in-degree distribution. ◁
  if  $\text{runif}(0, 1) < p$  then
     $i \leftarrow |G| + 1$ 
     $gp(i) \leftarrow g \in \{1, \dots, k\}$  uniformly at random.
  else
     $i \leftarrow i \in \{1, \dots, |G|\}$  with probability  $p_i \propto \text{in-degree}(i) + \delta_{in}$ 
  ▷ Then pick a gene (node)  $j$  to regulate  $i$ , proportional to the out-degree distribution, weighted by
  whether  $i$  is in the same group as  $j$ . ◁
   $j \leftarrow j \in \{1, \dots, |G|\}$  with probability  $p_j \propto (\text{out-degree}(j) + \delta_{out}) \times (w \text{ if } gp(i) = gp(j) \text{ else } 1)$ 
  ▷ Add the edge ( $j \rightarrow i$ ) to the graph. Note that  $j$  and  $i$  may be the same node, in which case we
  add the edge ( $j \rightarrow j$ );  $j$  and  $i$  may also already share the edge ( $j \rightarrow i$ ), in which case we add a
  duplicate edge. ◁
   $G \leftarrow (j \rightarrow i)$ 

```

130 modularity term w determine the fraction of edges which are drawn between members of the k
 131 groups – this fraction is approximately $w / (w + k - 1)$ (**Fig. 2B**). Finally, the bias terms δ_{in} and δ_{out}
 132 respectively control the coefficient of variation (CV) of the in- and out-degree distributions (**Fig.**
 133 **2B**). CV is the standard deviation of a distribution over its mean, and for power-law distributions
 134 the CV is related to the power-law coefficient: a larger CV means the distribution has a heavier tail
 135 (i.e. there are hub regulators which have many target genes; or there are hub target genes which
 136 are directly affected by many regulators).

137 2.3 Expression model

138 In order to enable reasonable comparisons with experimental data, we use an expression model
 139 with quantitative (rather than binary) measurements, and with dynamics subject to a non-linearity
 140 that enforces realistic physical constraints: gene expression is non-negative and saturates near a

141 maximum value. Given a graph structure generated using the algorithm above, we assign pa-
142 rameters to each gene (node) and regulatory interaction (edge) in the graph. Each gene i has two
143 rate parameters: one for innate RNA production in the absence of regulators (α_i), and another for
144 the decay of existing cellular RNAs (ℓ_i). Each regulatory relationship, between genes j and i , has
145 one parameter: a magnitude (β_{ji}) which describes the importance of the regulator for the expres-
146 sion of the target gene. We also enforce a constraint that interactions have a minimum strength
147 ($|\beta_{ji}| \geq 1$). A full description of the strategy we use to sample these parameters for synthetic
148 GRNs is in **Methods**.

149 Our expression model takes the form of a stochastic differential equation (SDE), and we pro-
150 duce expression values using forward simulation according to the Euler-Maruyama method (**Fig.**
151 **3A**). For gene i with regulators j having expression x_j (likewise x_i) at time t , the difference equation
152 for expression x'_i at time $t + \Delta t$ is given by

$$\frac{x'_i - x_i}{\Delta t} = \sigma(\alpha_i + \sum_j x_j \beta_{ji}) - \ell_i x_i + \mathcal{N}(0, s^2 \frac{x_i}{\Delta t}),$$

153 where the terms on the right hand side of the equation, in order, correspond to transcriptional
154 synthesis, degradation, and noise. Unless stated otherwise, we set $s = 10^{-4}$ as the magnitude of
155 noise, which serves to scale the intrinsic biological noise in synthesis and degradation of RNAs
156 (hence noise is also proportional to x_i). We let $\Delta t = 0.01$ be the step size, as in previous work [31],
157 and take $\sigma(x)$ as the logistic sigmoid (expit) function $\sigma(x) = 1/(1 + e^{-x})$. In practice, we conduct
158 forward simulation in vectorized form with an update rule:

$$x' = x + \Delta t \cdot (\sigma(\alpha + \beta^\top x) - \ell x) + \mathcal{N}(0, \Delta t \cdot s^2 \text{diag}(x)).$$

159 Throughout our experiments, we perform on the order of thousands of iterations and then check
160 that the system of differential equations has reached an expression steady-state (**Methods**).

161 Our model can be used to quantify the effects of many types of perturbations. These include
162 (1) gene knockouts (KOs), which we model by nullifying $x_j = 0$ (or equivalently, setting $\beta_{ji} = 0$ for
163 all i); (2) gene knockdown or overexpression, which can be modeled by decreasing or increasing
164 α_j , increasing or decreasing ℓ_j , or directly manipulating x_j to a fixed value; (3) enhancer edits or
165 transcriptional rewiring, modeled by changing specific β_{ji} ; and (4) changes to expression noise,
166 modeled by altering s , either globally or for specific genes. We further note that similarly for-
167 mulated perturbations with small magnitudes could also make appropriate models of the effects
168 of molecular quantitative trait loci (QTLs). Here, we focus solely on gene knockouts, which we
169 consider for the remainder of this work.

170 2.4 Perturbation studies

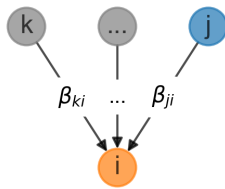
171 We conducted synthetic perturbation studies in 1,920 GRNs with $n = 2,000$ genes – these GRNs
172 were produced with a range of network generating parameters (**Methods**). For each GRN, we
173 initialized gene expression values at zero and conducted a minimum 5,000 iterations of forward
174 simulation, later verifying that the dynamical system reached equilibrium and assessing its stabil-
175 ity (**Fig. 3A,B, Methods**). We then independently knocked out each gene in the network and let
176 the system re-equilibrate after additional rounds of forward simulation (**Fig. 3B**). We computed

177 the effect of perturbing gene j as the log-fold change in expression x_i of all other genes i , which
 178 we refer to as the “perturbation effect” of gene j on gene i . Mathematically, this is

$$\log_2 FC_{ji} = \log_2(x_i | do(x_j = 0)) - \log_2(x_i)$$

179 where $x_i | do(x_j = 0)$ denotes the expression of gene i when gene j has been knocked out. While the
 180 majority of perturbation effects are small in all GRNs, with 86.6% of all effects below $|\log_2 FC| =$
 181 0.01, each network harbors a median 5,296 large effects on the order $|\log_2 FC| = 1$ (**Fig. 3C**). We
 182 also note substantial variability in the distribution of perturbation effects across networks (**Fig.**
 183 **3C**).

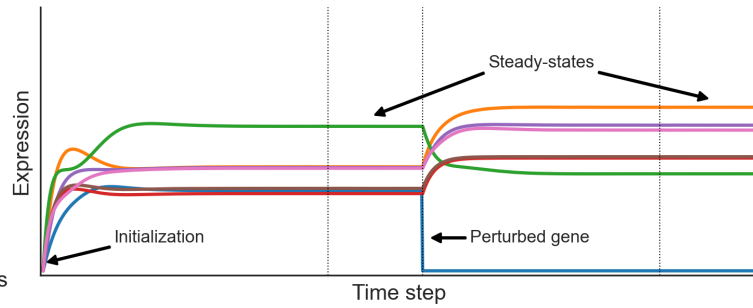
A: Model gene expression



Stochastic differential equation (SDE) has terms for synthesis, degradation, and noise for gene i at times $t, t+\Delta t$:

$$\frac{x_i^{[t+\Delta t]} - x_i^{[t]}}{\Delta t} = \sigma\left(\alpha_i + \sum_k \beta_{ki} x_k^{[t]}\right) - \ell_i x_i + s \sqrt{\frac{x_i^{[t]}}{\Delta t}} \mathcal{N}(0, 1)$$

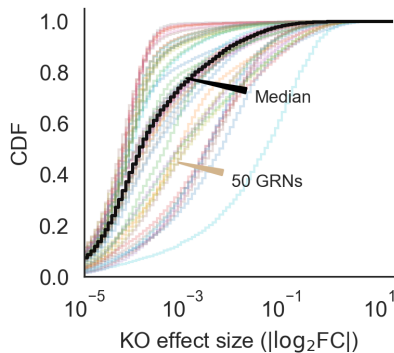
B: Compute gene knockout (KO) effects



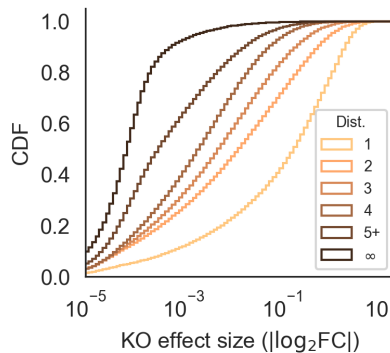
KO effect sizes are \log_2 fold-changes between expression steady-states:

$$\log_2 FC_{ji} = \log_2(x_i | do(x_j = 0)) - \log_2(x_i)$$

C: KO effects in 50 GRNs



D: KO effects by graph distance



E: KO effects by module

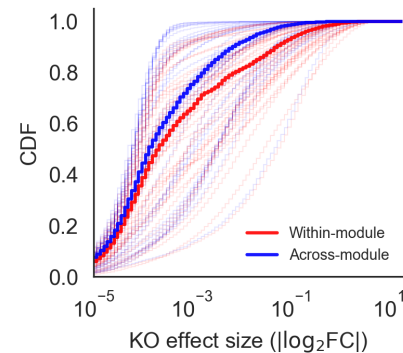


Figure 3: Perturbations and their effects within networks. (A) Overview of gene expression model and its parameters. Here, σ is the logistic sigmoid $\sigma(x) = 1/(1 + e^{-x})$. **(B)** Example forward simulation of the dynamical systems model. Trace lines show genes, whose expression values are initialized at zero. The system eventually reaches a steady-state, and is then subject to perturbation (knockout of gene j , i.e. holding $x_j = 0$). Further forward simulation leads to a new steady-state, from which we can compute perturbation effects ($\log_2 FC$ for other genes i). **(C)** Distribution of knockout (KO) effects (i.e., \log_2 fold-changes in expression x_i of a focal gene i) in 50 example GRNs, along with the median distribution (black line). **(D)** KO effects as a function of network distance between two genes, and **(E)** within and across modules given by the generating algorithm. Note that the solid lines in **(D)** and **(E)** are the median distributions over the 50 example GRNs, split respectively by distances and modules.

184 These effects are largely stratified by the distance between regulator and target (**Fig. 3D**), with

185 distance here being the length of the shortest path between genes along edges in the network.
186 Across GRNs, a majority of direct regulators of a gene confer at least a modest effect on average
187 (77.3% of genes at distance 1 have $|\log_2 \text{FC}| > 0.01$ when knocked out). Meanwhile, indirect
188 effects of this magnitude also exist, but are less common on a per-interaction basis (mean 21.5%
189 of gene pairs not connected by an edge). However, since mediation is much more common than
190 direct regulation, mediated effects contribute a substantial fraction of perturbation effects at all
191 but the largest magnitudes – for example, 98.5% of effects at $|\log_2 \text{FC}| > 0.01$ across GRNs are
192 mediated rather than direct (**Fig. S1**).

193 Since genes in the simulated GRNs belong to pre-defined groups, we further investigated the
194 extent to which perturbation effects cluster within rather than across groups. On average, there is
195 an enrichment of effects within groups – but as with the overall distribution, there is heterogeneity
196 in the distributions of within- and across-group perturbation effects (**Fig. 3E**). This heterogeneity
197 is driven largely by the modularity term: as w increases, the distributions of within- and across-
198 group effects become further separated, even across networks with different numbers of groups
199 (**Fig. S2**). This effect is based on changes in network architecture: since the strongest perturbation
200 effects are from direct regulators, an increased affinity for within-group regulation (i.e., larger w)
201 means that these effects should also come from members of the same group.

202 **2.5 Impact of network properties**

203 Next, we turned our attention to the relationship between properties of networks (as determined
204 by network generating parameters) and their distributions of perturbation effects. As a summary
205 of this distribution, we compared the number of genes which are hub KOs and hub target genes
206 in each of the 1,920 synthetic GRNs. We say a gene is a hub KO if it introduced a change of
207 $|\log_2 \text{FC}| > 0.1$ in at least 100 other genes when knocked out; analogously, we say a gene is a hub
208 target gene if its expression was changed by $|\log_2 \text{FC}| > 0.1$ upon knockout of at least 100 other
209 genes. Genes whose equilibrium expression was below the magnitude of noise were removed
210 from these counts, as their expression could vary widely across conditions solely due to noise. We
211 find that these statistics behave consistently with respect to the network generating parameters
212 across GRNs (**Fig. 4**), and that the directions of effect are also similar to the overall number of
213 perturbation effects at this threshold in the network (**Fig. S3**).

214 Graph sparsity has the greatest influence on the number of hub KOs and hub target genes in
215 the GRNs (**Fig. 4A**). More regulators per gene (large $1/p$) tends to translate to more perturbation
216 effects overall, increasing the number of both hub knockouts and target genes. Notably, the effects
217 on regulators and targets are not identical. In denser networks, the median number of hub KOs
218 tends to be larger than the number of hub target genes. However, in a subset of dense networks,
219 most genes in the network are identified as hub target genes. This is related to the absence of
220 stable equilibrium dynamics in the low-noise limit of the gene expression model (**Fig. S4**), which
221 suggests that as GRNs become more dense and genes are subject to regulation by larger fractions
222 of the network, the system is less likely to be stable. Although this term has a large effect on
223 perturbation effects, we find no obvious interaction between it and other terms in the generating
224 algorithm (**Fig. S5**).

225 GRNs with fewer groups (small k) and higher modularity (large w) tend to have fewer hub
226 KOs and hub target genes (**Figs. 4B, 4C**). The modularity term monotonically increases resilience

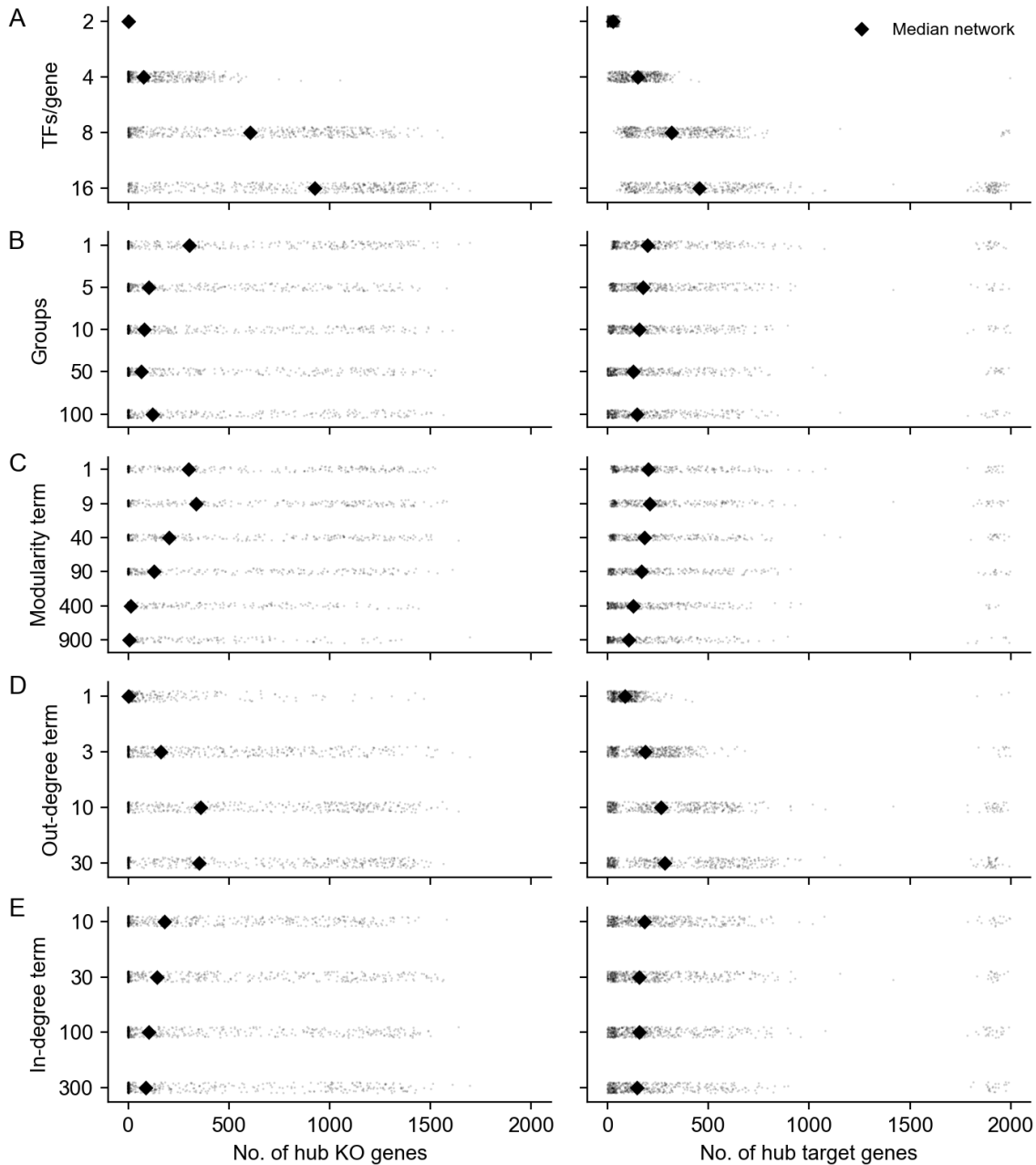


Figure 4: **Network properties influence the distribution of perturbation effects.** Counts of genes that are hub knockouts (**left**) and hub target genes (**right**) in each synthetic GRN, as a function of network generating parameters. Each panel shows all 1,920 GRNs as individual points, stratified by parameter values. Each distribution is annotated with its mean over GRNs (diamond points).

227 to perturbation; the group term monotonically decreases it, with the exception of $k = 1$. From
 228 the perspective of the network generating algorithm, $k = 1$ and $w = 1$ are identical; they are
 229 equivalent to the algorithm from Bollobas *et. al.*, 2003 [28] and correspond to the dissolution of
 230 modular structure with respect to the specified grouping. This is also equivalent to $k = 2000$, in
 231 which each gene in the network has its own group – this intuition is supported by the remaining

232 trend in (Fig. 4B). Meanwhile, in modular networks (large w), most edges are between members of
233 the same group. This might serve to confine the downstream effects of perturbations to members
234 of the same group, effectively dampening the transcriptional impact of altering the function of
235 master regulators.

236 When the out-degree distribution of GRNs has a heavier tail (small δ_{out}), there tend to be many
237 fewer hub knockout genes (Fig. 4D). This relationship is non-linear, and in the most extreme case
238 ($\delta_{out} = 1$) there are only 89 hub KOs on average (median 1 hub KO) in the GRN. This effect is
239 a consequence of preferential attachment; as more edges are drawn from master regulators, out-
240 going regulatory effects also concentrate there as well. Counterintuitively, this parameter exerts
241 influence over the number of hub target genes in the network as well, and in the same direction.
242 When effects are concentrated among a few key regulators, it may simply be less feasible for any
243 gene to be affected by many knockouts since there are fewer genes that have many knockout ef-
244 fects at all. As with the sparsity term, we do not see obvious interactions between this term and
245 others in the generating algorithm (Fig. S6). Meanwhile, when the in-degree distribution of GRNs
246 has a less heavy tail (large δ_{in}), there are modestly more hub target genes and hub KOs (Fig. 4E).
247 The source of this trend is difficult to intuit, but the effect is very weak.

248 Looking across parameters, these results reflect a wide range of variation in the susceptibility
249 of GRNs to perturbations as a function of their structural properties. While there is substantial
250 overlap in the distributions of hub KO and target genes across network generating parameters,
251 we find that all parameters except the in-degree term have statistically significant effects on both
252 quantities ($p < 0.001$ for all tests, Fig. S7 – full results in Tables S1, S2). We estimate these effects
253 with a multiple regression on the logit-transformed fraction of genes in each GRN which are hub
254 KOs or hub target genes (Methods). In total, the network generating parameters explain just un-
255 der half the variance in the fraction of the GRN which is either a hub KO (model $r^2 = 0.59$) or hub
256 target gene (model $r^2 = 0.46$). Moreover, there is also a noteworthy thematic consistency across
257 parameters. In all cases, the direction of protective effect from perturbation is also the direction
258 of biological plausibility with respect to our modeling desiderata, where intuition dictates that
259 GRNs should be sparse, modular, and have a heavy-tailed out- but not in-degree distribution.

260 2.6 Comparing with experimental data

261 With this intuition about network properties in hand, we now return to real experimental data.
262 Given that synthetic GRNs with quantifiably different structures produce qualitatively different
263 distributions of knockout effects, we next sought to ask whether any of them were also similar to
264 real data. For this, we made use of the subset of perturbations that correspond one-to-one with
265 gene expression readout in a recent Perturb-seq study [9].

266 We compared the real and synthetic data using their cumulative distributions of perturbation
267 effects, computed both from the perspective of genes as regulators and as targets of regulation
268 (Fig. 5A-B). Since these data have different numbers of genes that are not lowly expressed, we
269 normalized the number of incoming and outgoing effects to the size of the network (Methods). In
270 the Perturb-seq data, we find noticeable qualitative differences between the distribution of incom-
271 ing and outgoing effects – these differences are consistent with the notion that GRNs should have
272 master regulators, but not master target genes. In the synthetic data, we find substantial diversity
273 in both distributions across GRNs, including many patterns that seem wholly incompatible with

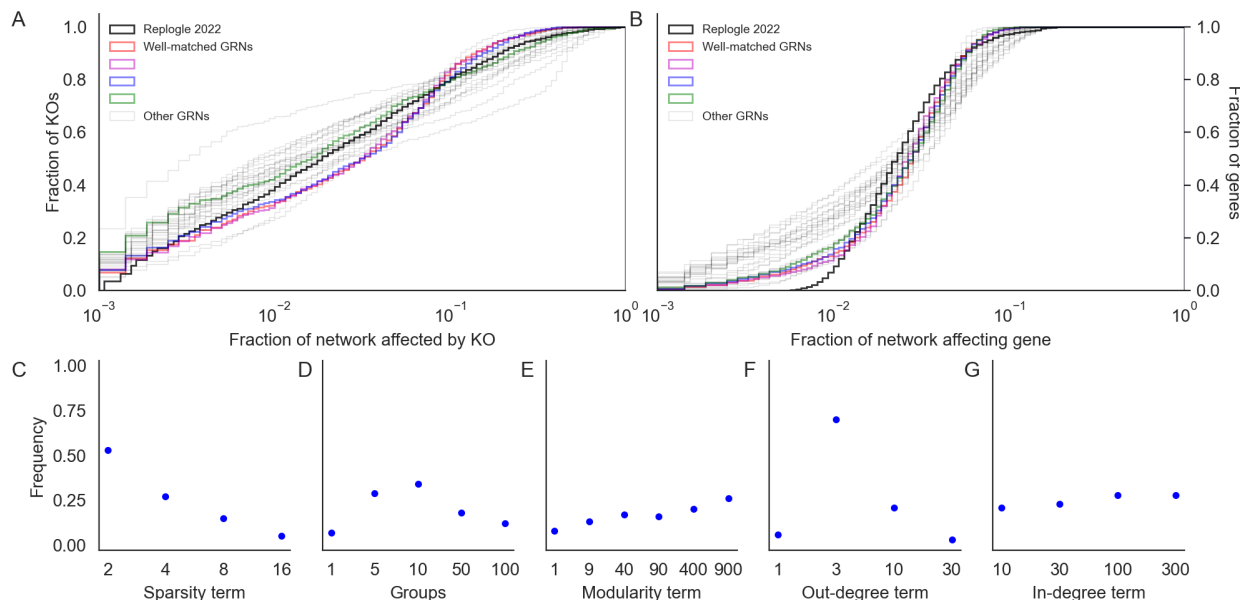


Figure 5: **Comparing with genome-wide Perturb-seq.** Fraction of GRN that (A) affects each gene when perturbed (outgoing effects) or (B) is affected by other perturbations (incoming effects). In synthetic data, perturbation effects are thresholded at the top 3% of absolute log-fold change values, matching the proportion of pairwise tests from the Perturb-seq data with FDR-corrected Anderson-Darling $p < 0.05$. Highlighted in color are the four GRNs that best match the Perturb-seq data. (C-G) Distribution of network generating parameters for the 100 GRNs that are best matched to Perturb-seq data (by Kolmogorov-Smirnov p -value rank for both distributions in A and B).

274 those observed in experiments. Meanwhile, some GRNs seem well-matched to the Perturb-seq
 275 results: the distributions closest to the data are highlighted in color in Fig. 5A-B, and correspond
 276 to those having the smallest Kolmogorov-Smirnov test statistics when compared with the data
 277 distributions (Methods).

278 Although the focus of our work is not network inference, we do observe a coherent set of
 279 properties among the well-matched networks (Fig. 5C-G). Specifically, they share a relatively
 280 small number of regulators per gene (two, rather than 16); they have a small number of groups
 281 (five to ten rather than one or 100); they are highly modular (large w); and they have a heavy
 282 tail in the distribution of out-degree but not in-degree (δ_{out} near three but δ_{in} on the order of
 283 100). Consistent with previous results, we find these parameter sets to be within a range that
 284 matches our motivating intuition about the structural properties of GRNs, and we do not find
 285 these properties to have obvious pairwise interactions that affect concordance to data (Fig. S8).

286 2.7 Challenges and opportunities for inference

287 Finally, we highlight the utility of our simulation approach by considering the value of different
 288 data sources for inference tasks. For this, we conducted further analysis using an example syn-
 289 thetic GRN whose patterns of knockout effects were well-matched with Perturb-seq data. Specif-
 290 ically, we focused on the recovery of edges, edge weights, and group structure using interven-
 291 tional data (e.g., perturbation effects) and observational data (e.g., coexpression). We made use

292 of perturbation effects as previously described, and further computed pairwise gene coexpression
293 values using additional rounds of forward simulation from the expression model at steady state
294 to approximate the naturally occurring variation across cells (**Methods**).

295 **2.7.1 Discovering pairwise relationships**

296 Several computational and experimental approaches have been used to estimate pairwise causal
297 relationships between genes, with the ultimate goal of wholesale inference of gene regulatory net-
298 works [10, 11]. These data and methods are broad in scope, and range from estimating networks
299 using natural variation in gene expression values from bulk tissue [12, 23] to fitting complex ma-
300 chine learning models on data from single-cell perturbation experiments [7, 15, 32]. Here, we
301 consider two descriptive pairwise summary statistics at the gene level – gene coexpression across
302 cells and perturbation effects across gene knockouts – and their connections to edges in a simu-
303 lated GRN.

304 In the synthetic data, we find that the distributions of pairwise gene coexpression values and
305 knockout effects both span multiple orders of magnitude (**Fig. 6**). However, where the distribution
306 of knockout effects differs dramatically between gene pairs that share an edge and those that do
307 not, the distributions of coexpression values have substantial overlap (**Fig. 6A,B**). This difference
308 in distribution reflects what each statistic tends to measure. Gene perturbation effects tend to
309 flow through the network along edges, and are therefore highly related to the network distance
310 between genes (**Fig. 3D**). As a special case, this includes whether or not two genes share a direct
311 regulatory relationship in the form of an edge. Meanwhile, strong coexpression is more often due
312 to co-regulation than to there being a direct causal relationship between genes (**Fig. S9**).

313 For gene pairs where there is direct regulation we see that both knockout effects (**Fig. 6C**) and
314 coexpression (**Fig. 6D**) have weak correlation with the strength of known regulatory relationships.
315 This reflects that both statistics are imperfect measures of regulatory importance: they are both
316 affected by differences in regulatory architecture across genes (e.g., number of regulators or the
317 intensity of transcriptional buffering). We further see this when directly comparing coexpression
318 and knockout effects between pairs of genes. Across all pairs of genes, these two statistics are
319 uncorrelated – but the two are highly correlated among pairs of genes that share an edge (**Fig.**
320 **6E**). In this way, both perturbation effects and coexpression contain similar information about
321 edges in the GRN – but coexpression also measures non-causal relationships between genes, like
322 coregulation, and is therefore systematically uncorrelated with perturbation effects even in real
323 data (**Fig. S10**).

324 Together, these results underscore the importance of interventional data for inferring network
325 edges. They also highlight limitations in the use of coexpression networks. But neither form of
326 data are a panacea, and care is warranted in the analysis of experimental data and in the develop-
327 ment of structure learning algorithms. For example, sorting and thresholding perturbation effects
328 has been shown to be a high-quality baseline for network reconstruction [10, 11] (one that we also
329 use to compare networks in **Fig. 5**). However, false negative effects can arise when regulatory
330 effects are weak due to transcriptional buffering, and false positive edges can be drawn where
331 effects are amplified by mediation. This suggests that structure learning algorithms could benefit
332 from modeling the transcriptional state of individual genes (i.e., level of buffering at baseline) and
333 from approaches to explicitly resolve direct versus mediated effects.

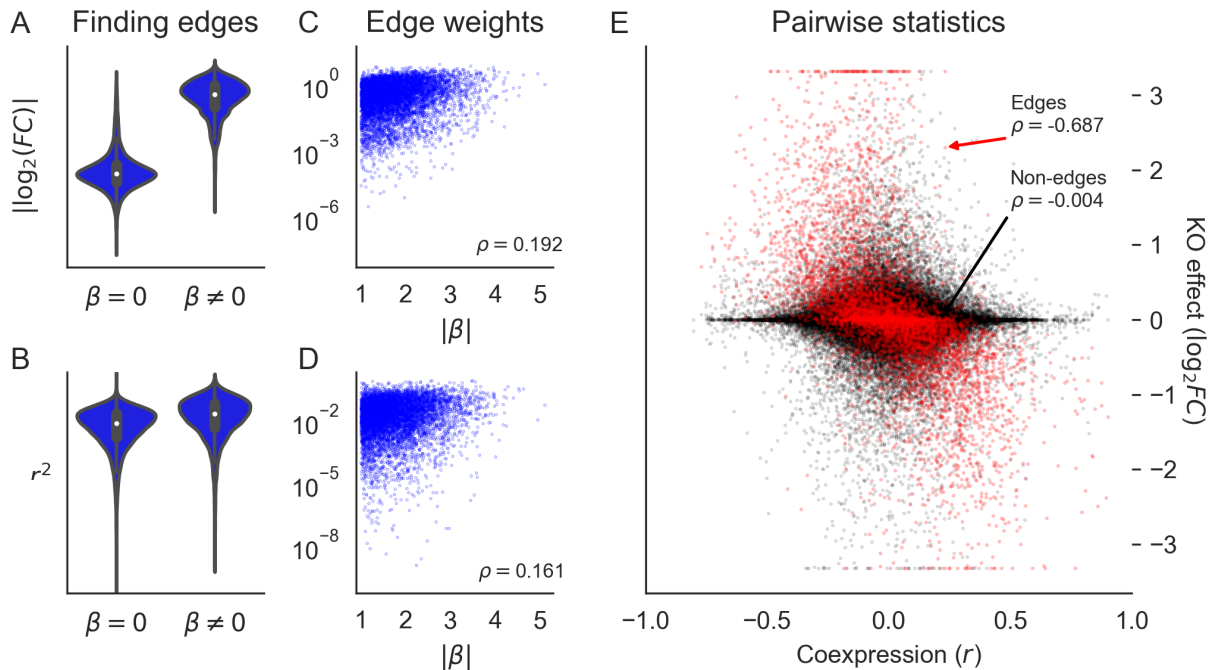


Figure 6: **Perturbations more reliably measure fine-scale network structure than coexpression.** (A) Distribution of perturbation effects between pairs of genes in a realistic synthetic GRN that do or do not share an edge. (B) Rank correlation of perturbation effect sizes with edge weights. (C) Distribution of gene coexpression between pairs of genes that do or do not share an edge. (D) Rank correlation of coexpression magnitude with edge weights. (E) Rank correlation between coexpression and perturbation effects (the y -axis is clipped at values corresponding to tenfold change).

334 2.7.2 Discovering group structure

335 Recent work has also attempted to identify trait-relevant sets of genes that act through coordinated
 336 effects in a particular cell type. These groups are sometimes called programs, and it is common to
 337 use dimensionality reduction techniques like singular value decomposition (SVD) or non-negative
 338 matrix factorization (NMF) on single-cell expression values to identify groups [8, 33]. In our ex-
 339 ample synthetic GRN and in the Perturb-seq data, we used a variant of this approach based on
 340 truncated SVD (TSVD) to assign genes to programs. As input, we used the set of 75,328 unperturbed
 341 cells from real data [9] and downsamples of the entire experiment to the same number
 342 of cells; for the synthetic data, we simulated the same number of cells from baseline or baseline
 343 and perturbed conditions, mimicking the composition of the real experiments. From these data,
 344 we computed the first 200 singular vectors of the expression data, using each vector to define a
 345 “program” of 100 genes with the largest loadings (Methods).

346 Here, we assess the extent to which these programs and their constituent singular vectors
 347 replicate across experiments from perturbed and unperturbed conditions. We use canonical cor-
 348 relation analysis (CCA) to assess the similarity of the singular vectors. This technique seeks to
 349 find rotations a, b of inputs x, y such that the correlation between $a^\top x$ and $b^\top y$ is maximized –
 350 the transformed inputs are called canonical variables, and we report their correlations when the
 351 inputs x, y are gene singular vectors from different experimental conditions (Fig. 7A). In the syn-

352 thetic GRN, the canonical correlation steadily declines over the 200 dimensions of input. Notably,
 353 the magnitude of this correlation is similar when perturbation data are compared to a replicate or
 354 to unperturbed data. Even though this correlation is modest by the 100th set of canonical vari-
 355 ables, this trend suggests consistency between lower-dimensional representations of expression
 356 data regardless of cell state (perturbed or unperturbed).

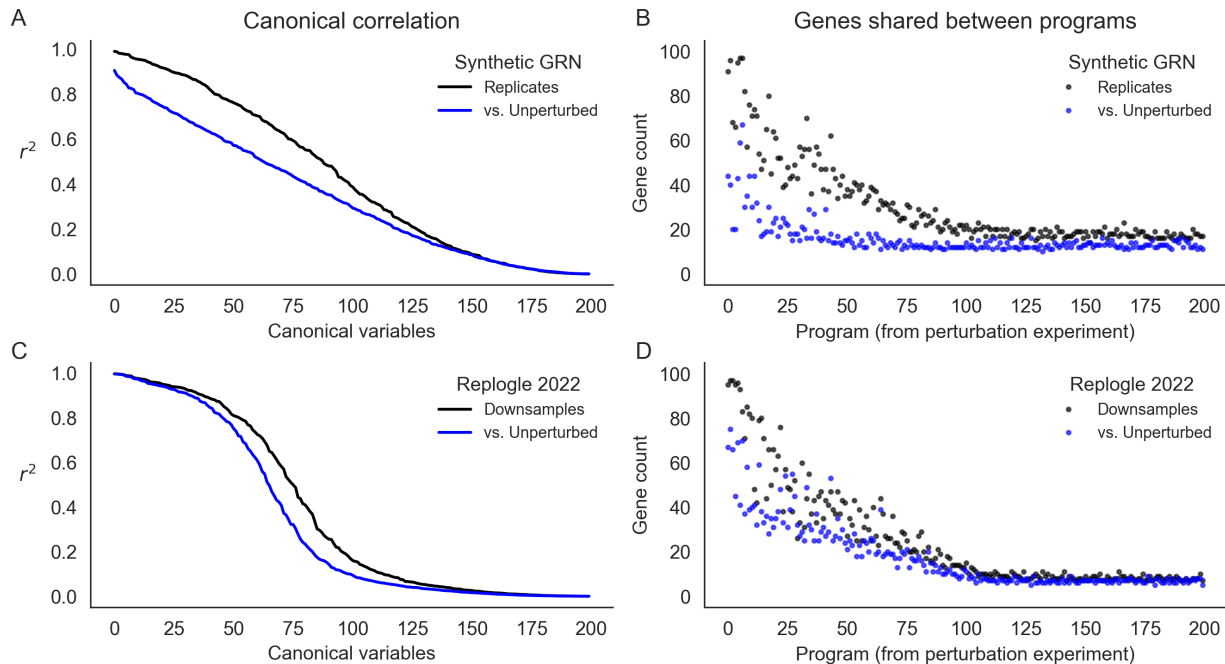


Figure 7: Learned representations are similar between control and intervened-upon cells. Concordance between low-rank representations of single cells in a simulated GRN (top row) and downsamples of experimental data (Replogle *et. al.*, 2022). **(A)** Correlation between the first 200 canonical variables (linear combinations of singular vectors) between samples of 75,328 baseline or baseline+perturbed cells from a synthetic GRN. **(B)** Overlap in gene programs inferred from singular value decomposition of single cell expression data. Programs are defined using singular vectors of gene expression from perturbed cells (x-axis), and intersected with programs analogously defined from baseline and additional perturbed cells. **(C)** Canonical correlation of control cells and two downsamples of the entire Perturb-seq experiment (Replogle *et. al.*, 2022). **(D)** Overlap in gene programs computed from control and downsamples of experimental Perturb-seq data.

357 At this sample size (75,238 cells) for the synthetic GRN, however, there is a difference in the re-
 358 producibility of individual programs across data sources (perturbed or unperturbed; **Fig. 7B**). For
 359 this, we compare programs computed from one perturbation experiment (the “reference”) to pro-
 360 grams from a replicate perturbation experiment and to programs from unperturbed cells. For each
 361 program from the reference, we report the maximum number of genes which overlap any other
 362 program computed from each of the other data sources. The first few programs (corresponding
 363 to the first few singular vectors) are highly reproducible in the replicate perturbation data. This
 364 overlap steadily declines to no effective overlap after the first ~100 programs. Despite similar
 365 canonical correlation, the unperturbed data do not replicate the same programs to the same extent
 366 – there is modest overlap with the first few programs from the perturbation data, and this overlap
 367 decays very quickly (after the first ~20 programs). When assessing these programs with respect

368 to the ($k = 10$) ground truth groups of this network, we find that nearly all true groups are at
369 least modestly well represented by the top 50 programs from both data sources. However, the
370 programs from the perturbation data much better represent the true groups than those from the
371 unperturbed data (**Fig. S11**).

372 We find similar results in the experimental Perturb-seq data. Here, however, the first few
373 canonical variables are highly correlated, and the canonical correlation drops off precipitously be-
374 tween the 50th and 100th canonical variables (**Fig. 7C**). We also find that programs computed from
375 two downsamples of the entire experiment are about as reproducible as those from the simulated
376 data, but are slightly more similar to the programs from control cells (**Fig. 7D**). While this may
377 reflect some aspect of GRN structure, it is also related to the number of cells in the input data and
378 magnitude of intrinsic gene expression noise. Both tend to reduce canonical correlations and the
379 reproducibility of gene programs. In the real data, lowering the number of cells input to TSVD
380 lowers both canonical correlation and program similarity compared to the entire experiment; re-
381 latedly, we find that the 75,328 control cells exhibit comparable performance as 30,000 perturbed
382 cells at recovering representations from the full data (**Fig. S12**). In the synthetic networks, we find
383 that altering the level of global transcriptional noise (s) alters the concordance between replicates
384 and between perturbed and unperturbed cell states – at high levels of noise, there is little practical
385 difference between programs derived from perturbed or unperturbed cells, but with low levels of
386 noise, the programs from perturbation data are markedly different (**Fig. S13**). For presentation in
387 **Fig. 7A-B**, we chose a level of noise ($s = 0.3$) that recapitulated the qualitative behavior of the real
388 data.

389 Taken together, these findings seem to suggest that the leading variance components of single-
390 cell gene expression data will be similar across perturbed and unperturbed conditions, unless the
391 magnitude of perturbation effects is greater than the level of intrinsic transcriptional noise. Re-
392 latedly, we suspect that dimensionality reduction techniques will produce concordant represen-
393 tations of both perturbed and unperturbed data under similar conditions, and that this similarity
394 can propagate into gene sets derived from these representations. This begs a key line of questions
395 for future work: where, and how, do molecular perturbations add value in uncovering the sets of
396 genes that are collectively important for cell-type and disease-specific processes? In light of the
397 number of cells required for reliable inference at this scale, we anticipate that large atlas-style cell
398 reference data (e.g., the Human Cell Atlas and similar resources [34–36]) may provide a critical
399 opportunity to reveal global aspects of network structure.

400 3 Discussion

401 In this work, we have presented a new model to simulate gene regulatory networks, with par-
402 ticular emphasis on generating networks with realistic structural properties. We note that this
403 algorithm may be of interest in contexts outside gene regulation – namely, in any study of scale-
404 free networks with group-like structure. We also anticipate that our technique to simulate gene
405 expression from arbitrary networks may be useful for model development and benchmarking, or
406 in other studies where network structures are known or may be hypothesized.

407 Here, we have highlighted the utility of our approach with simulations to develop intuition
408 about key properties of GRNs, particularly in the context of molecular perturbations and coexpres-

409 sion data. While our study design draws inspiration from recent works using Perturb-seq, we also
410 acknowledge limitations to the realism of our model. In focusing on the equilibrium dynamics of
411 cells of one type, we have ignored developmental trajectories and cell-type heterogeneity within
412 tissues, both of which modify our assumptions about regulatory network structure. For the sake of
413 computational efficiency in quantifying expression for thousands of genes, we have also eschewed
414 detailed models of the biological synthesis and experimental measurement of cellular RNAs: in
415 future work where it is critical to match distributions of count data from experiments, we encour-
416 age modeling these complexities. Similar considerations may also be necessary for the application
417 of our approach beyond modeling knockouts – for example, in studying genetic variation which
418 affects gene expression.

419 Independently, our results suggest that the space of realistic network structures may be quite
420 limited, and that it may be useful to consider this prior information in various inference settings.
421 While our approach as outlined in this work is not optimized for inference, the algorithms we
422 describe are generative, which means they could be used directly in applications for simulation-
423 based inference. Although we used experimental data from K562 cells in this study, we anticipate
424 the high-level structural properties of GRNs will generalize across different cell types. Moreover,
425 we observed through simulations that hallmark properties of GRNs tend to confer resilience to
426 perturbations across multiple measures, reducing the number of sensitive target genes and large-
427 effect master regulators. We do not suspect this is an incidental finding in light of the selection
428 to which GRNs are subject over evolutionary time, and suspect that considering this type of con-
429 straint may be insightful for future work.

430 Looking forward, we also anticipate that broad observational studies of diverse cell types and
431 deep interventional studies of specific cell lines will both be useful in disentangling the basis of
432 complex traits in regulatory networks. However, a key question remains in determining how best
433 to leverage these data types towards a unifying understanding of cell biology. We suggest that
434 a scaffolded approach to this problem may be useful. Where the scale of cell atlases presents a
435 unique opportunity to learn transferable representations of cells across developmental states and
436 tissues, perhaps including the discovery of cellular programs, these data are limited in their ability
437 to resolve interactions between single genes. This is where perturbation data – however limited
438 to specific cell types – retain critical value. Even as existing network inference algorithms expe-
439 rience computational challenges in genome-scale applications, the modularity of GRNs suggests
440 that piecewise inference strategies may be viable until these challenges are resolved. As efforts
441 like these enhance our mechanistic understanding of biological networks, we hope that our work
442 serves to provide general intuition on their salient structural properties. We are optimistic that
443 understanding these principles will be useful for an array of challenges and highlight future op-
444 portunities in functional genomics.

445 **4 Acknowledgements**

446 We would like to thank Mineto Ota, Emma Dann, Courtney Smith, Garyk Brixi, Josh Weinstock,
447 and members of the Pritchard Lab at Stanford University for helpful comments and discussion
448 related to this work. M.A. acknowledges support from a Microsoft Research PhD Fellowship,
449 and from the National Library of Medicine (NLM) under training grant T15LM007033. This
450 work was supported by the National Human Genome Research Institute (NHGRI) under grants
451 R01HG008140 and U01HG012069 (J.K.P.) and by the National Institute of General Medical Sci-
452 ences (NIGMS) under grant R01GM115889 (G.S.).

453 5 Methods

454 5.1 Graph generating parameters

455 5.1.1 Sampling

456 A full description of the graph generating algorithm can be found in the main text, with the exact
457 procedure given by **Algorithm 1**. Here, we provide additional intuition on its generating param-
458 eters, and detail the scheme for sampling them.

459 In motivating our study, we highlight several key properties of gene regulatory networks:
460 briefly, these are sparsity, modular groups, and asymmetric power-law degree distributions. In
461 **Fig. 2** we show that these properties are individually tuned by parameters of our generating
462 algorithm. When generating synthetic networks, we sample values for each parameter across one
463 to three orders of magnitude. To cover these ranges, the values are spaced geometrically, and the
464 extrema are chosen to overlap values which we believe to be consistent with biological intuition
465 for a network of $n = 2,000$ genes.

- 466 • Sparsity term p : $\{\frac{1}{2}, \frac{1}{4}, \frac{1}{8}, \frac{1}{16}\}$.
- 467 • Number of groups k : $\{1, 5, 10, 50, 100\}$.
- 468 • Modularity term w : $\{1, 9, 40, 90, 400, 900\}$.
- 469 • In-degree uniformity term δ_{in} : $\{10, 30, 100, 300\}$.
- 470 • Out-degree uniformity term δ_{out} : $\{1, 3, 10, 30\}$.

471 The sparsity term p is sampled so that the average number of regulators per gene spans from
472 low single-digits to low double-digits. The number of groups is sampled from $k = 100$, which
473 corresponds to a rough lower limit on the size of groups (20 genes), to $k = 1$, which corresponds
474 to the dissolution of group structure and is equivalently to the algorithm from Bollobas *et. al.*,
475 2003 [28]. The modularity / within-group affinity term w is sampled in a similar way: $w = 1$ also
476 corresponds to the dissolution of group structure, again giving the algorithm from Bollobas *et. al.*,
477 2003, and $w = 900$ gives an upper limit on modularity with respect to groups k . The in- and out-
478 degree uniformity terms δ_{in} , δ_{out} are both sampled across orders of magnitude. The bounds for
479 the in-degree term to be larger in magnitude, corresponding to the assumption that the in-degree
480 distribution should be less dispersed (i.e., have fewer hubs) than the out-degree distribution, but
481 the range of values is intentionally overlapping.

482 To produce the set of 1,920 GRNs used in the study, we simulated one network with every
483 possible combination of parameters listed above: this totals $4 \times 5 \times 6 \times 4 \times 4 = 1,920$ networks.

484 5.1.2 Relationship to perturbation effects

485 We performed a regression analysis to estimate the effect of each graph generating parameter on
486 the distribution of perturbation effects in the synthetic GRNs. Specifically, we regressed the logit-
487 transformed fraction of genes in each GRN that are hub regulators or hub targets according to the

488 following equation:

$$\text{logit}(p_{\text{genes}}) \sim 1 + (1/p) + k' + w + \delta_{in} + \delta_{out},$$

489 where $1/p$ is the inverse of the sparsity term, k' is a transformed number of groups (GRNs with
490 $k = 1$ group are treated as GRNs with $k = n = 2000$ groups; see **Fig. 4**), and w , δ_{in} , and δ_{out} are as
491 described above. The dependent variable of the regression, p_{genes} is either the fraction of genes in
492 the GRN which are hub regulators or hub targets. These quantities are analyzed separately. Full
493 results for each regression are in **Table S1** and **S2**.

494 5.2 Expression simulation

495 5.2.1 Parameter selection

496 An overview of our gene expression model can be found in the main text. Here, we describe
497 the sampling strategy for the parameters of the model and give additional information on their
498 interpretation. Recall that the expression, x_i , of gene i is influenced by the following variables:

- 499 • the baseline transcription rate, α_i ,
- 500 • the degradation rate of RNAs, ℓ_i ,
- 501 • effects from regulating genes, β_{ji} ,
- 502 • expression noise, with magnitude s .

503 Note that α and ℓ are properties of genes (nodes); β is a property of regulatory interactions (edges);
504 and s is a global parameter for the entire network. During forward simulation from the discretized
505 stochastic differential equation, we take steps of size $\Delta t = 0.01$ as in prior work [31], and update
506 expression values from x (at time t) to x' (at time $t + \Delta t$) according to the following:

$$x' = x + \Delta t \cdot (\sigma(\alpha + \beta x) - \ell x) + s\sqrt{\Delta t \cdot x}\mathcal{N}(0, I).$$

507 In the deterministic limit, this results in an equation satisfied by any potential steady-state

$$x^* = \sigma(\alpha + \beta x^*) / \ell,$$

508 where $\sigma(x) = \frac{1}{1+e^{-x}}$ is the logistic sigmoid. When setting up the model given a graph structure
509 from our generating algorithm, we simulate expression parameters according to the following
510 scheme:

- 511 • $\sigma(\alpha_i) \stackrel{\text{iid}}{\sim} \text{Beta}(2, 8)$, under the assumption that genes have low but non-zero expression at
512 baseline, in the absence of regulation – i.e., $\sigma(\alpha_i)$ is small. Here, $\sigma(x) = \frac{1}{1+e^{-x}}$ is again the
513 logistic sigmoid (expit) function.
- 514 • $\ell_i \stackrel{\text{iid}}{\sim} \text{Beta}(8, 2)$, under the assumption that the maximum expression of each gene, $1/\ell_i$, tends
515 to be of a similar order of magnitude (close to one), but can vary. To prevent steady-state
516 gene expression from being excessively large (by having small ℓ_i), we hard clip ℓ_i to be at
517 least as large as $e^{-\alpha_i}$.

- 518 • $\beta_{ji} \stackrel{\text{iid}}{\sim} (2p_j - 1) \cdot (1 + \text{Half-Normal}(0, 1))$, under the assumptions that regulatory interactions
 519 have a minimum strength ($|\beta_{ji}| \geq 1$). Here, $p_j \stackrel{\text{iid}}{\sim} \text{Bernoulli}(p = 0.8)$ is the probability that a
 520 regulator j acts as an activator rather than a repressor.
- 521 • $s = 10^{-4}$, fixed across all genes in the networks. This value is chosen to be as large as possible
 522 without limiting detection of very small KO effects. At this level of noise, we can reliably
 523 detect \log_2 fold-changes down to the order of 10^{-4} (**Fig. 3D**).

524 5.2.2 Forward simulation

525 Once parameters of the expression model are chosen for a specific GRN, we initialize the expres-
 526 sion of each gene $x_i = 0$ and conduct forward simulation according to the update rule given in
 527 the previous section, which is also described in the main text.

528 When performing forward simulations, we initialize all genes in the network to have zero
 529 expression. We then perform $b = 5,000$ iterations of forward simulation as a “burn-in”. After
 530 burn-in, we check whether the system of equations has converged to a steady-state by measuring
 531 differences in the time averaged mean after the burn-in. Specifically, we compute the maximum
 532 absolute \log_2 fold-change of non-lowly expressed genes in the network

$$\max_{g, \bar{x}_{g,i} > s} \log_2 \left(\frac{\bar{x}_{g,i}}{\bar{x}_{g,i-h}} \right)$$

533 where g indexes genes whose running mean expression $\bar{x}_{g,i}$ at the current iteration i is above the
 534 noise magnitude s , and h is the step size to check for convergence. Mathematically, the running
 535 mean in the numerator is

$$\bar{x}_{g,i} = \frac{1}{i-b} \sum_{t=b}^i x_{g,t}$$

536 where $x_{g,t}$ is the expression of gene g at iteration t . The denominator $\bar{x}_{g,i-h}$ is analogously the
 537 running mean expression of gene g the last time we checked for convergence.

$$\bar{x}_{g,i-h} = \frac{1}{i-h-b} \sum_{t=b}^{i-h} x_{g,t}$$

538 If this maximum log fold-change is below 10^{-3} , we say the system has converged, and take the
 539 vector \bar{x}_i as the steady-state expression of all genes in the network. We perform this check every
 540 $h = 1,000$ iterations, up to a maximum $t_{max} = 20,000$ iterations. We take the vector $\bar{x}_{t_{max}}$ as an
 541 approximate equilibrium state if the system did not fully converge.

542 We further assess the stability of the steady-state of each GRN by performing a linear stability
 543 analysis of the expression model in the limit $s \rightarrow 0$. In this limit, the expression model takes the
 544 form of an ordinary differential equation (ODE). The stability of an equilibrium point \bar{x} of this
 545 ODE can be assessed using the eigenvalues of the Jacobian matrix J evaluated at \bar{x} – if all of the
 546 eigenvalues have a negative real part, the system is said to be stable [37]. Here, we have

$$J = \left\{ \frac{\partial f(x_i)}{\partial x_j} \right\}_{ij}$$

547 where the (i, j) th entries correspond to the partial derivative of the deterministic part of the ex-
548 pression function $f(x_i)$ of gene i , with respect to the expression x_j of gene j . For our model,

$$\begin{aligned}\frac{\partial f(x_i)}{\partial x_j} &= \frac{\partial}{\partial x_j} (\sigma(\alpha_i + \sum_k \beta_{ki} x_k) - \ell_i x_i) \\ &= \beta_{ji} \sigma(\alpha_i + \sum_k \beta_{ki} x_k) [1 - \sigma(\alpha_i + \sum_k \beta_{ki} x_k)] - \mathbb{1}(i = j) \ell_i\end{aligned}$$

549 where the first term is zero for $\beta_{ji} = 0$ and the second term is zero for $j \neq i$.

550 5.2.3 Perturbation experiments

551 For each synthetic GRN in this study, we perform a systematic assessment of gene-level perturba-
552 tion effects. We start with baseline steady-state expression values of an instantiated GRN, with
553 edges drawn according to the generating algorithm and expression parameters chosen as de-
554 scribed above. Then, separately for each gene j , we perform a knockout by setting $\beta_{ji} = 0$ for
555 all other genes i – that is, we nullify its outgoing effects. This perturbs the equilibrium dynamics
556 of the expression SDE, and we conduct additional rounds of forward simulation using the mod-
557 ified parameters until a new expression steady-state is reached. We perform the same procedure
558 with burn-in and convergence checks as in the previous section.

559 We summarize the effect that perturbing gene j has on gene i using a log fold-change in ex-
560 pression values:

$$\log_2 \text{FC}_{ji} = \log_2(x_i | \text{do}(x_j = 0)) - \log_2(x_i)$$

561 where x_i is the steady-state expression of gene i under baseline conditions, and $x_i | \text{do}(x_j = 0)$ is its
562 steady-state expression when gene j has been perturbed (both computed as described above).

563 5.2.4 Baseline coexpression

564 Since gene coexpression is also commonly used to describe pairwise relationships between genes,
565 we further use the expression SDE to compute the gene-level correlations at steady-state in the
566 synthetic GRNs. Under baseline conditions, we perform $t = 10,000$ additional forward time steps,
567 from which we sample $m = 10,000$ “baseline cells” by taking the gene expression value at every
568 step. The noise inherent to the model ($s = 10^{-4}$) produces sufficient variability in this cell popu-
569 lation to compute gene-level correlations. We measure the coexpression of genes all i and j (not
570 filtering out lowly expressed genes) using the Pearson correlation between x_i and x_j across cells.

571 5.3 Perturb-seq data

572 5.3.1 Data processing

573 To motivate aspects of our work, and to assess our simulations in context of experimental data,
574 we make use of summary statistics from a recent genome-scale Perturb-seq study [9]. Specifi-
575 cally, we used pairwise FDR-corrected Anderson-Darling p-values (from the supplemental file,
576 "anderson-darling p-values, BH-corrected.csv.gz") as a measure of the expression response
577 to single-gene perturbations. Throughout this work, we used a single large subset of these data

578 corresponding to the set of genes whose expression was subject to both experimental perturba-
579 tion and measurement in response. We matched perturbations to target genes using the provided
580 ENSEMBL gene IDs, subsetting to perturbations which targeted any primary transcript. In (rare)
581 cases where there was more than one such perturbation, we used the perturbation which induced
582 a statistically significant change in the expression of the target transcript. We note that target genes
583 with expression levels below 0.25 UMI per cell were not included in this file, which further limited
584 the genes included in our analysis. We performed a similar post-processing step when analyzing
585 results from the synthetic networks, limiting analysis to genes whose steady-state expression was
586 above the level of intrinsic noise (i.e., $x_i > s$).

587 5.3.2 Comparing with simulations

588 We compared the distribution of perturbation effects (incoming and outgoing) at the gene level
589 when assessing similarities between the real and simulated networks. For this, we thresholded
590 pairwise effects from the experimental data at FDR-corrected Anderson-Darling $p < 0.05$, saying
591 that effects at this significance level constitute biologically meaningful effects, and others do not.
592 At this threshold, we find that 3.16% of pairwise effects are called significant. For a given gene i ,
593 we then computed two values: the fraction of the network that is affected when i is perturbed (i.e.,
594 the fraction of genes j for which $p_{ij} < 0.05$), and the fraction of the network that affects i when
595 perturbed (i.e., the fraction of genes j for which $p_{ji} < 0.05$).

596 We then compared these distributions to analogous quantities derived from the synthetic
597 GRNs. Since the experimental data are affected by imperfect statistical power, we set the dis-
598 covery rate to be equal across all synthetic GRNs, doing so by taking the top 3.16% of pairwise
599 perturbation effects (i.e., $|\log_2 \text{FC}|_{ji} > k$, where k varies) as “statistically significant”. For each
600 gene i in a synthetic GRN, we computed the fraction of the network which is affected when i is
601 perturbed (i.e., the fraction of genes j for which $|\log_2 \text{FC}|_{ij} > k$), and the fraction of the network
602 which affects i when perturbed (i.e., the fraction of genes j for which $|\log_2 \text{FC}|_{ji} > k$). Note that
603 in each GRN in **Fig. 5**, we remove lowly-expressed genes, with baseline expression $x_i < s$. This
604 means that the number of genes analyzed is not exactly the same for all GRNs – we therefore nor-
605 malized the distribution of perturbation effects by the number of genes that are included in the
606 analysis (i.e., those not lowly-expressed).

607 Finally, we compared the distributions of incoming and outgoing perturbation effects using
608 the Kolmogorov-Smirnov test as implemented in `scipy` (`scipy.stats.ks_2samp`) [38]. This is a
609 nonparametric test for equality of distribution between two samples, which measures the maxi-
610 mum difference between cumulative distribution functions. To select the synthetic GRNs which
611 are closest to the real data, we rank GRNs by largest KS p -values with each distribution (incom-
612 ing and outgoing), then find the smallest rank r such that k GRNs are in the top r of all GRNs
613 compared to both distributions.

614 5.4 Gene programs

615 5.4.1 Truncated singular value decomposition

616 We used truncated singular value decomposition (TSVD) to cluster genes into “programs” based
617 on their expression profiles in cells from both perturbed and unperturbed settings, using the
618 `TruncatedSVD` function from `scikit-learn` [39]. Briefly, TSVD is an algorithmic modification of
619 singular value decomposition (SVD), which produces orthogonal singular vectors corresponding
620 to the directions of maximum variance in the input data. In TSVD, only the top k vectors are
621 computed, which results in faster computational runtimes for our analysis.

622 We assembled separate input datasets consisting of perturbed and unperturbed cells for both
623 synthetic data and using downsamples of the experimental Perturb-seq data. For the synthetic
624 data, we simulated 75,328 single cells from baseline conditions by forward simulation from the
625 expression fixed point of the GRN, sampling cells from every forward time step. We also sim-
626 ulated the expression of an identical number of cells under perturbed conditions, modeling the
627 split of cells after the real Perturb-seq study: roughly 8.1% of the cells corresponded to baseline
628 conditions, and the remainder were assigned uniformly at random to a knockout condition for
629 each of the 2,000 genes in the GRN (this corresponds to 35 cells per KO on average). We do not
630 filter out lowly expressed genes for this analysis.

631 For the real data, we used single-cell expression data of the 5,247 genes in our data subset
632 from all 75,328 control cells as measurements of the GRN in unperturbed conditions. Then, to
633 avoid effects from varying the size of the input cell population, we performed two independent
634 (random) downsamples of the entire experiment to the same number of cells as measurements of
635 the GRN in perturbed conditions.

636 With each of these input datasets X , we normalized each gene to have zero mean and unit vari-
637 ance, and then performed TSVD to compute the top $k = 200$ dimensions of expression variability.
638 This resulted in singular matrices for cells (U) and genes (V), and a diagonal matrix of singular
639 values, S . The product of these matrices approximates the input:

$$X \approx USV^T$$

640 and we used the gene loadings (columns v of the gene singular matrix V) to define gene programs.
641 Each “program” corresponds one-to-one with one of the gene singular vectors v , and is the set of
642 100 genes with the largest squared entries of v .

643 5.4.2 Similarity across datasets

644 We assess the similarity of gene programs from two different experiments in two distinct ways:
645 one using the set of genes which constitutes each program, and the other using the singular vector
646 used to define it. When comparing programs $\{p_i\}$ from one (reference) experiment to programs
647 $\{p'_j\}$ from another experiment, we report the maximum overlap between each program p_i in the
648 reference set to *any* program p'_j in other set – that is,

$$\text{overlap}(p_i, \{p'_j\}) = \max_j |p_i \cap p'_j|$$

649 which quantifies the extent to which each program is reproduced by the other experiment. When
650 comparing gene singular vectors $V = \{v_i\}$, $V' = \{v'_j\}$ from the two experiments, we make use of
651 the fact that the SVD of their dot product is a well-characterized mathematical procedure called
652 canonical correlation analysis (CCA) [40]. The top k components of this decomposition are called
653 canonical variables, and they each represent the axes of rotation which maximize correlation be-
654 tween variables in the input data. Here, we report the canonical correlation (singular values from
655 the second SVD step) for the first 200 canonical variables, to quantify the extent to which the
656 lower-dimensional representations of the inputs are consistent with one another.

657 References

- 658 [1] Efthymia Papalexi and Rahul Satija. Single-cell RNA sequencing to explore immune cell
659 heterogeneity. *Nature Reviews Immunology*, 18(1):35–45, January 2018. Publisher: Nature Pub-
660 lishing Group.
- 661 [2] Gioele La Manno, Ruslan Soldatov, Amit Zeisel, Emelie Braun, Hannah Hochgerner, Viktor
662 Petukhov, Katja Lidschreiber, Maria E. Kastrioti, Peter Lönnerberg, Alessandro Furlan, Jean
663 Fan, Lars E. Borm, Zehua Liu, David van Bruggen, Jimin Guo, Xiaoling He, Roger Barker,
664 Erik Sundström, Gonçalo Castelo-Branco, Patrick Cramer, Igor Adameyko, Sten Linnarsson,
665 and Peter V. Kharchenko. RNA velocity of single cells. *Nature*, 560(7719):494–498, August
666 2018. Publisher: Nature Publishing Group.
- 667 [3] Volker Bergen, Marius Lange, Stefan Peidli, F. Alexander Wolf, and Fabian J. Theis. General-
668 izing RNA velocity to transient cell states through dynamical modeling. *Nature Biotechnology*,
669 38(12):1408–1414, December 2020. Publisher: Nature Publishing Group.
- 670 [4] Atray Dixit, Oren Parnas, Biyu Li, Jenny Chen, Charles P. Fulco, Livnat Jerby-Arnon, Ne-
671 manja D. Marjanovic, Danielle Dionne, Tyler Burks, Raktima Raychowdhury, Britt Adamson,
672 Thomas M. Norman, Eric S. Lander, Jonathan S. Weissman, Nir Friedman, and Aviv Regev.
673 Perturb-Seq: Dissecting Molecular Circuits with Scalable Single-Cell RNA Profiling of Pooled
674 Genetic Screens. *Cell*, 167(7):1853–1866.e17, December 2016.
- 675 [5] Joseph M. Replogle, Thomas M. Norman, Albert Xu, Jeffrey A. Hussmann, Jin Chen, J. Zach-
676 ery Cogan, Elliott J. Meer, Jessica M. Terry, Daniel P. Riordan, Niranjan Srinivas, Ian T. Fiddes,
677 Joseph G. Arthur, Luigi J. Alvarado, Katherine A. Pfeiffer, Tarjei S. Mikkelsen, Jonathan S.
678 Weissman, and Britt Adamson. Combinatorial single-cell CRISPR screens by direct guide
679 RNA capture and targeted sequencing. *Nature Biotechnology*, 38(8):954–961, August 2020.
680 Publisher: Nature Publishing Group.
- 681 [6] Jacob W. Freimer, Oren Shaked, Sahin Naqvi, Nasa Sinnott-Armstrong, Arwa Kathiria, Chris-
682 tian M. Garrido, Amy F. Chen, Jessica T. Cortez, William J. Greenleaf, Jonathan K. Pritchard,
683 and Alexander Marson. Systematic discovery and perturbation of regulatory genes in human
684 T cells reveals the architecture of immune networks. *Nature Genetics*, 54(8):1133–1144, August
685 2022. Number: 8 Publisher: Nature Publishing Group.
- 686 [7] Joshua S. Weinstock, Maya M. Arce, Jacob W. Freimer, Mineto Ota, Alexander Marson, Alexis
687 Battle, and Jonathan K. Pritchard. Gene regulatory network inference from CRISPR pertur-
688 bations in primary CD4+ T cells elucidates the genomic basis of immune disease. *bioRxiv*,
689 page 2023.09.17.557749, October 2023.
- 690 [8] Gavin R. Schnitzler, Helen Kang, Shi Fang, Ramcharan S. Angom, Vivian S. Lee-Kim, X. Rosa
691 Ma, Ronghao Zhou, Tony Zeng, Katherine Guo, Martin S. Taylor, Shamsudheen K. Vel-
692 larikkal, Aurelie E. Barry, Oscar Sias-Garcia, Alex Bloemendal, Glen Munson, Philine Guckel-
693 berger, Tung H. Nguyen, Drew T. Bergman, Stephen Hinshaw, Nathan Cheng, Brian Cleary,
694 Krishna Aragam, Eric S. Lander, Hilarly K. Finucane, Debabrata Mukhopadhyay, Rajat M.
695 Gupta, and Jesse M. Engreitz. Convergence of coronary artery disease genes onto endothelial
696 cell programs. *Nature*, 626(8000):799–807, February 2024. Number: 8000 Publisher: Nature
697 Publishing Group.

- 698 [9] Joseph M. Replogle, Reuben A. Saunders, Angela N. Pogson, Jeffrey A. Hussmann, Alexan-
699 der Lenail, Alina Guna, Lauren Mascibroda, Eric J. Wagner, Karen Adelman, Gila Lithwick-
700 Yanai, Nika Iremadze, Florian Oberstrass, Doron Lipson, Jessica L. Bonnar, Marco Jost,
701 Thomas M. Norman, and Jonathan S. Weissman. Mapping information-rich genotype-
702 phenotype landscapes with genome-scale Perturb-seq. *Cell*, 185(14):2559–2575.e28, July 2022.
- 703 [10] Mathieu Chevalley, Jacob Sackett-Sanders, Yusuf Roohani, Pascal Notin, Artemy Bakulin,
704 Dariusz Brzezinski, Kaiwen Deng, Yuanfang Guan, Justin Hong, Michael Ibrahim, Wojciech
705 Kotlowski, Marcin Kowiel, Panagiotis Misiakos, Achille Nazaret, Markus Püschel, Chris
706 Wendler, Arash Mehrjou, and Patrick Schwab. The CausalBench challenge: A machine
707 learning contest for gene network inference from single-cell perturbation data, August 2023.
708 arXiv:2308.15395 [cs, q-bio].
- 709 [11] Mathieu Chevalley, Yusuf Roohani, Arash Mehrjou, Jure Leskovec, and Patrick Schwab.
710 CausalBench: A Large-scale Benchmark for Network Inference from Single-cell Perturbation
711 Data, July 2023. arXiv:2210.17283 [cs].
- 712 [12] Nir Friedman, Michal Linial, Iftach Nachman, and Dana Pe’er. Using Bayesian networks to
713 analyze expression data. In *Proceedings of the fourth annual international conference on Com-
714 putational molecular biology*, RECOMB ’00, pages 127–135, New York, NY, USA, April 2000.
715 Association for Computing Machinery.
- 716 [13] David Heckerman. A Tutorial on Learning with Bayesian Networks. In Dawn E. Holmes
717 and Lakhmi C. Jain, editors, *Innovations in Bayesian Networks: Theory and Applications*, pages
718 33–82. Springer, Berlin, Heidelberg, 2008.
- 719 [14] Yuhao Wang, Liam Solus, Karren Dai Yang, and Caroline Uhler. Permutation-based Causal
720 Inference Algorithms with Interventions, November 2017. arXiv:1705.10220 [stat].
- 721 [15] Romain Lopez, Jan-Christian Hütter, Jonathan K. Pritchard, and Aviv Regev. Large-Scale
722 Differentiable Causal Discovery of Factor Graphs, October 2022. arXiv:2206.07824 [cs, q-bio,
723 stat].
- 724 [16] Douglas Yao, Loic Binan, Jon Bezney, Brooke Simonton, Jahanara Freedman, Chris J. Frang-
725 ieh, Kushal Dey, Kathryn Geiger-Schuller, Basak Eraslan, Alexander Gusev, Aviv Regev, and
726 Brian Cleary. Scalable genetic screening for regulatory circuits using compressed Perturb-seq.
727 *Nature Biotechnology*, pages 1–14, October 2023. Publisher: Nature Publishing Group.
- 728 [17] R. Milo, S. Shen-Orr, S. Itzkovitz, N. Kashtan, D. Chklovskii, and U. Alon. Network Mo-
729 tifs: Simple Building Blocks of Complex Networks. *Science*, 298(5594):824–827, October 2002.
730 Publisher: American Association for the Advancement of Science.
- 731 [18] Shai S. Shen-Orr, Ron Milo, Shmoolik Mangan, and Uri Alon. Network motifs in the tran-
732 scriptional regulation network of *Escherichia coli*. *Nature Genetics*, 31(1):64–68, May 2002.
733 Publisher: Nature Publishing Group.
- 734 [19] C. Seshadhri, Aneesh Sharma, Andrew Stolman, and Ashish Goel. The impossibility of low-
735 rank representations for triangle-rich complex networks. *Proceedings of the National Academy
736 of Sciences*, 117(11):5631–5637, March 2020. Publisher: Proceedings of the National Academy
737 of Sciences.

- 738 [20] S. Balaji, Lakshminarayan M. Iyer, L. Aravind, and M. Madan Babu. Uncovering a Hidden
739 Distributed Architecture Behind Scale-free Transcriptional Regulatory Networks. *Journal of*
740 *Molecular Biology*, 360(1):204–212, June 2006.
- 741 [21] Mark B. Gerstein, Anshul Kundaje, Manoj Hariharan, Stephen G. Landt, Koon-Kiu Yan, Chao
742 Cheng, Xinmeng Jasmine Mu, Ekta Khurana, Joel Rozowsky, Roger Alexander, Renqiang
743 Min, Pedro Alves, Alexej Abyzov, Nick Addleman, Nitin Bhardwaj, Alan P. Boyle, Philip
744 Cayting, Alexandra Charos, David Z. Chen, Yong Cheng, Declan Clarke, Catharine Eastman,
745 Ghia Euskirchen, Seth Fretze, Yao Fu, Jason Gertz, Fabian Grubert, Arif Harmanci, Preti Jain,
746 Maya Kasowski, Phil Lacroute, Jing Leng, Jin Lian, Hannah Monahan, Henriette O’Geen,
747 Zhengqing Ouyang, E. Christopher Partridge, Dorrelyn Patacsil, Florencia Pauli, Debasish
748 Raha, Lucia Ramirez, Timothy E. Reddy, Brian Reed, Minyi Shi, Teri Slifer, Jing Wang, Linfeng
749 Wu, Xinqiong Yang, Kevin Y. Yip, Gili Zilberman-Schapira, Serafim Batzoglou, Arend Sidow,
750 Peggy J. Farnham, Richard M. Myers, Sherman M. Weissman, and Michael Snyder. Architec-
751 ture of the human regulatory network derived from ENCODE data. *Nature*, 489(7414):91–100,
752 September 2012. Publisher: Nature Publishing Group.
- 753 [22] Arun J. Singh, Stephen A. Ramsey, Theresa M. Filtz, and Chrissa Kioussi. Differential
754 gene regulatory networks in development and disease. *Cellular and Molecular Life Sciences*,
755 75(6):1013–1025, March 2018.
- 756 [23] Peter Langfelder and Steve Horvath. WGCNA: an R package for weighted correlation net-
757 work analysis. *BMC Bioinformatics*, 9(1):559, December 2008.
- 758 [24] Paul W. Holland, Kathryn Blackmond Laskey, and Samuel Leinhardt. Stochastic blockmod-
759 els: First steps. *Social Networks*, 5(2):109–137, June 1983.
- 760 [25] Thorben Funke and Till Becker. Stochastic block models: A comparison of variants and infer-
761 ence methods. *PLOS ONE*, 14(4):e0215296, April 2019. Publisher: Public Library of Science.
- 762 [26] Albert-László Barabási and Réka Albert. Emergence of Scaling in Random Networks. *Science*,
763 286(5439):509–512, October 1999. Publisher: American Association for the Advancement of
764 Science.
- 765 [27] Petter Holme and Beom Jun Kim. Growing scale-free networks with tunable clustering. *Physi-
766 cal Review E*, 65(2):026107, January 2002. Publisher: American Physical Society.
- 767 [28] Béla Bollobás, Christian Borgs, Jennifer T Chayes, and Oliver Riordan. Directed scale-free
768 graphs. In *SODA*, volume 3, pages 132–139, 2003.
- 769 [29] Duncan J. Watts and Steven H. Strogatz. Collective dynamics of ‘small-world’ networks.
770 *Nature*, 393(6684):440–442, June 1998. Publisher: Nature Publishing Group.
- 771 [30] Reuven Cohen and Shlomo Havlin. Scale-Free Networks Are Ultrasmall. *Physical Review
772 Letters*, 90(5):058701, February 2003. Publisher: American Physical Society.
- 773 [31] Payam Dibaenia and Saurabh Sinha. SERGIO: A Single-Cell Expression Simulator Guided
774 by Gene Regulatory Networks. *Cell Systems*, 11(3):252–271.e11, September 2020.
- 775 [32] Xun Zheng, Bryon Aragam, Pradeep Ravikumar, and Eric P. Xing. DAGs with NO TEARS:
776 Continuous Optimization for Structure Learning, November 2018. arXiv:1803.01422 [cs, stat].

- 777 [33] Dylan Kotliar, Adrian Veres, M Aurel Nagy, Shervin Tabrizi, Eran Hodis, Douglas A Melton,
778 and Pardis C Sabeti. Identifying gene expression programs of cell-type identity and cellular
779 activity with single-cell RNA-Seq. *eLife*, 8:e43803, July 2019. Publisher: eLife Sciences
780 Publications, Ltd.
- 781 [34] Aviv Regev, Sarah A Teichmann, Eric S Lander, Ido Amit, Christophe Benoist, Ewan Birney,
782 Bernd Bodenmiller, Peter Campbell, Piero Carninci, Menna Clatworthy, Hans Clevers, Bart
783 Deplancke, Ian Dunham, James Eberwine, Roland Eils, Wolfgang Enard, Andrew Farmer,
784 Lars Fugger, Berthold Göttgens, Nir Hacohen, Muzlifah Haniffa, Martin Hemberg, Seung
785 Kim, Paul Klenerman, Arnold Kriegstein, Ed Lein, Sten Linnarsson, Emma Lundberg, Joakim
786 Lundeberg, Partha Majumder, John C Marioni, Miriam Merad, Musa Mhlanga, Martijn Naw-
787 ijn, Mihai Netea, Garry Nolan, Dana Pe'er, Anthony Phillipakis, Chris P Ponting, Stephen
788 Quake, Wolf Reik, Orit Rozenblatt-Rosen, Joshua Sanes, Rahul Satija, Ton N Schumacher,
789 Alex Shalek, Ehud Shapiro, Padmanee Sharma, Jay W Shin, Oliver Stegle, Michael Stratton,
790 Michael J T Stubbington, Fabian J Theis, Matthias Uhlen, Alexander van Oudenaarden, Al-
791 lon Wagner, Fiona Watt, Jonathan Weissman, Barbara Wold, Ramnik Xavier, Nir Yosef, and
792 Human Cell Atlas Meeting Participants. The Human Cell Atlas. *eLife*, 6:e27041, December
793 2017. Publisher: eLife Sciences Publications, Ltd.
- 794 [35] THE TABULA SAPIENS CONSORTIUM. The Tabula Sapiens: A multiple-organ, single-cell
795 transcriptomic atlas of humans. *Science*, 376(6594):eabl4896, May 2022. Publisher: American
796 Association for the Advancement of Science.
- 797 [36] Colin Megill, Bruce Martin, Charlotte Weaver, Sidney Bell, Lia Prins, Seve Badajoz, Brian Mc-
798 Candless, Angela Oliveira Pisco, Marcus Kinsella, Fiona Griffin, Justin Kiggins, Genevieve
799 Haliburton, Arathi Mani, Matthew Weiden, Madison Dunitz, Maximilian Lombardo, Timmy
800 Huang, Trent Smith, Signe Chambers, Jeremy Freeman, Jonah Cool, and Ambrose Carr. cel-
801 lXgene: a performant, scalable exploration platform for high dimensional sparse matrices,
802 April 2021. Pages: 2021.04.05.438318 Section: New Results.
- 803 [37] Steven H Strogatz. *Nonlinear dynamics and chaos: with applications to physics, biology, chemistry,*
804 *and engineering*. CRC press, 2018.
- 805 [38] Pauli Virtanen, Ralf Gommers, Travis E. Oliphant, Matt Haberland, Tyler Reddy, David
806 Cournapeau, Evgeni Burovski, Pearu Peterson, Warren Weckesser, Jonathan Bright, Stéfan J.
807 van der Walt, Matthew Brett, Joshua Wilson, K. Jarrod Millman, Nikolay Mayorov, An-
808 drew R. J. Nelson, Eric Jones, Robert Kern, Eric Larson, C. J. Carey, İlhan Polat, Yu Feng,
809 Eric W. Moore, Jake VanderPlas, Denis Laxalde, Josef Perktold, Robert Cimrman, Ian Hen-
810 riksen, E. A. Quintero, Charles R. Harris, Anne M. Archibald, Antônio H. Ribeiro, Fabian
811 Pedregosa, and Paul van Mulbregt. SciPy 1.0: fundamental algorithms for scientific com-
812 puting in Python. *Nature Methods*, 17(3):261–272, March 2020. Publisher: Nature Publishing
813 Group.
- 814 [39] Fabian Pedregosa, Gaël Varoquaux, Alexandre Gramfort, Vincent Michel, Bertrand Thirion,
815 Olivier Grisel, Mathieu Blondel, Peter Prettenhofer, Ron Weiss, Vincent Dubourg, et al. Scikit-
816 learn: Machine learning in python. *the Journal of machine Learning research*, 12:2825–2830, 2011.
- 817 [40] William H Press. Canonical correlation clarified by singular value decomposition, 2011.

818 Supplementary Information

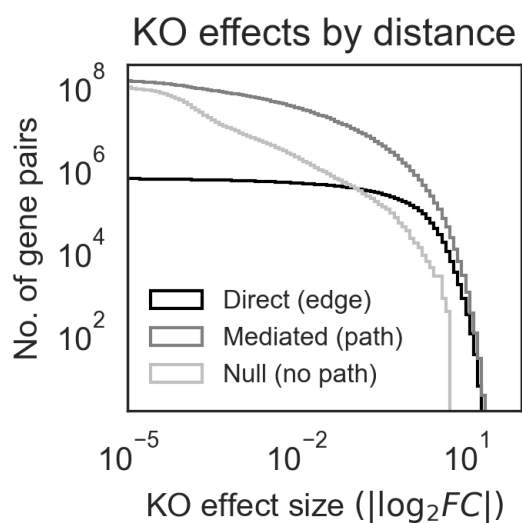


Figure S1: Mediated effects outnumber direct effects at most magnitudes. Same as Fig. 3D, but with distances binned by whether pairs of genes are connected by an edge (distance 1, a “direct effect”), any path (distance greater than 1, a “mediated effect”), or no path at all (“null”). Note also that the y -axis is the count of gene pairs with a perturbation effect of at least the magnitude given on the x -axis – that is, the distribution shown is a non-normalized inverse CDF. Gene pairs are pooled from the 50 example GRNs in Fig. 3.

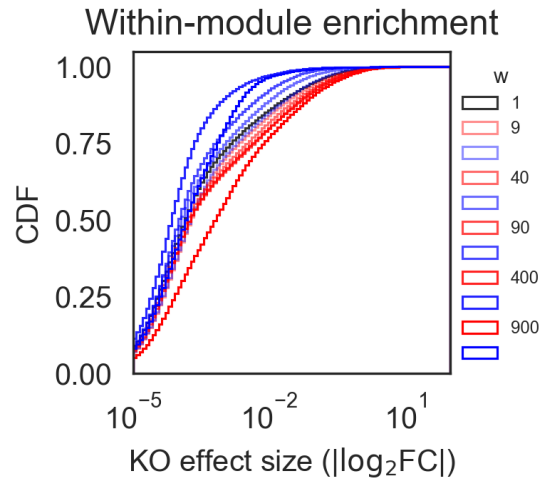


Figure S2: Modularity term differentiates within- and between-module effects. Same as Fig. 3E, with within-module perturbation effects in red and between-module perturbation effects in blue. Here, networks are chosen so as to highlight the effect of the modularity term w . Each pair of blue and red tracelines is distribution of the within- (red) or across-module perturbation effects a single GRN. The generating parameters for these GRNs vary w (see legend) but hold other parameters constant, as follow: $p = 1/4$, $k = 50$, $\delta_{in} = 10$, $\delta_{out} = 10$.

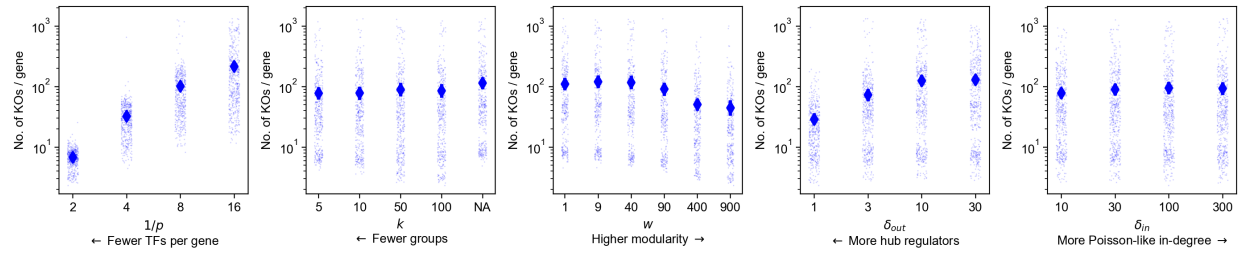


Figure S3: Network generating parameters affect the number of KO effects. Same as Fig. 4, but with summary statistic (y -axis) as the average number of perturbation effects per gene in the GRN with $|\log_2 FC| \geq 0.1$. We observe a similar direction of effect for each parameter as with the statistics presented in the main text.

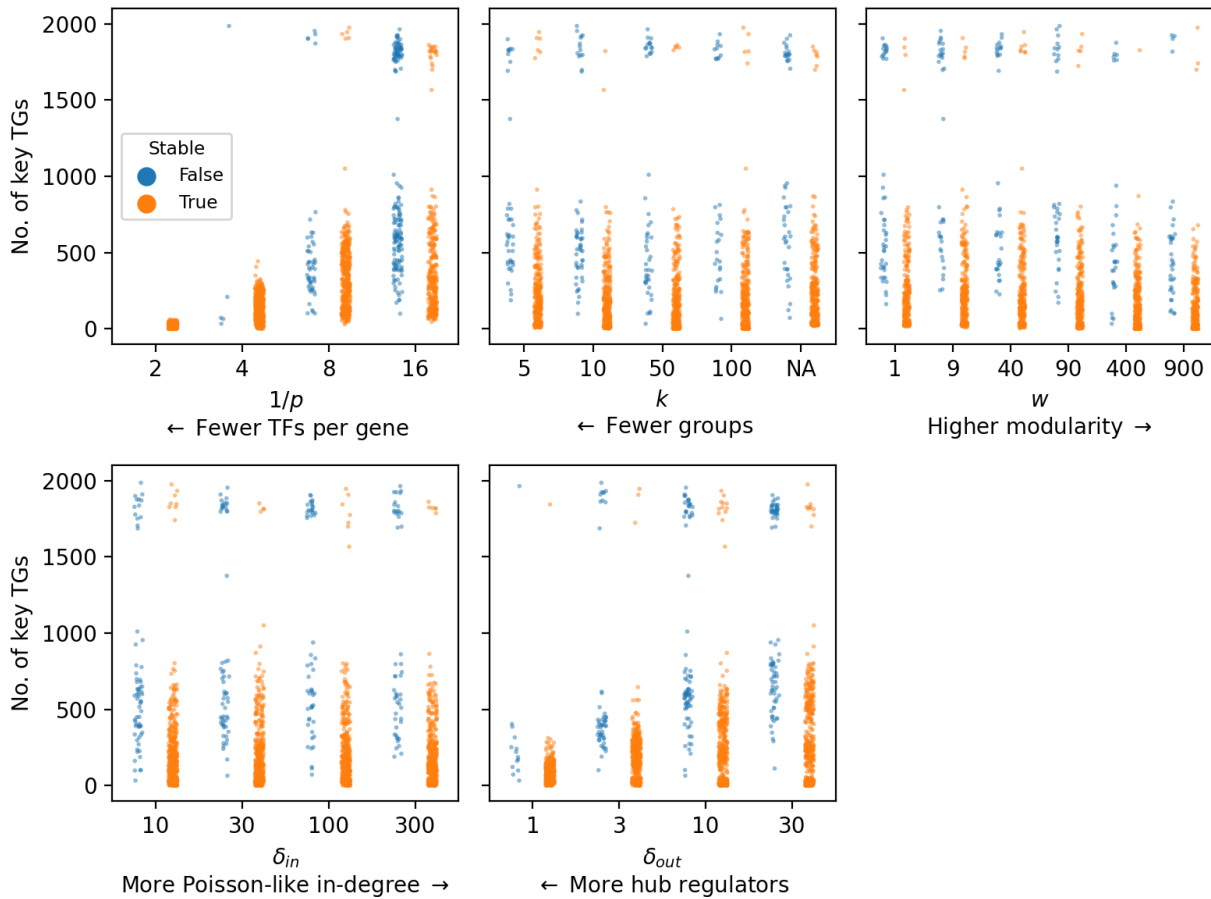


Figure S4: Network generating parameters affect the stability of the fixed point. Same as Fig. 4, only showing the number of key target genes and stratifying by whether the expression equilibrium point of the synthetic GRN is stable (**Methods**). In all, 1,693 of the 1,920 GRNs (88.2%) reach an expression equilibrium through forward simulation of the SDE which is a stable fixed point of the corresponding ODE. These GRNs tend to be sparse (lower $1/p$), modular (higher w), and have more hub regulators (lower δ_{out}).

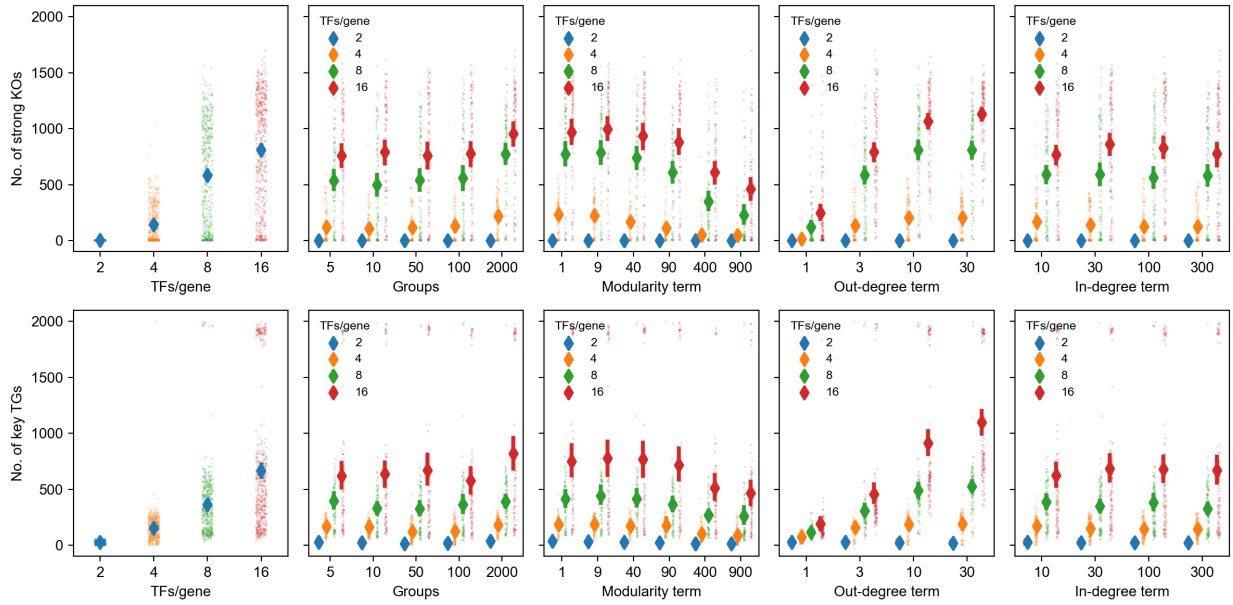


Figure S5: No interaction between sparsity term and other network generating parameters. Same as Fig. 4, but with additional stratification by the sparsity term $1/p$. There is no obvious visual evidence for interactions between the parameters.

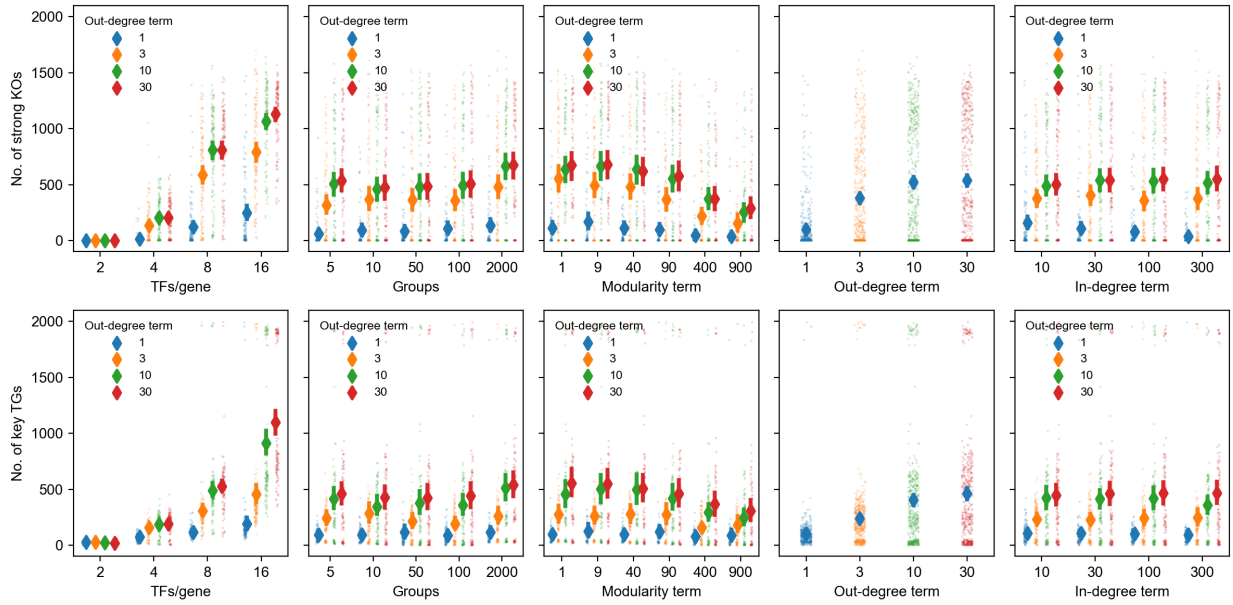


Figure S6: No interaction between out-degree term and other network generating parameters. Same as Fig. 4, but with additional stratification by the out-degree term δ_{out} . There is no obvious visual evidence for interactions between the parameters.

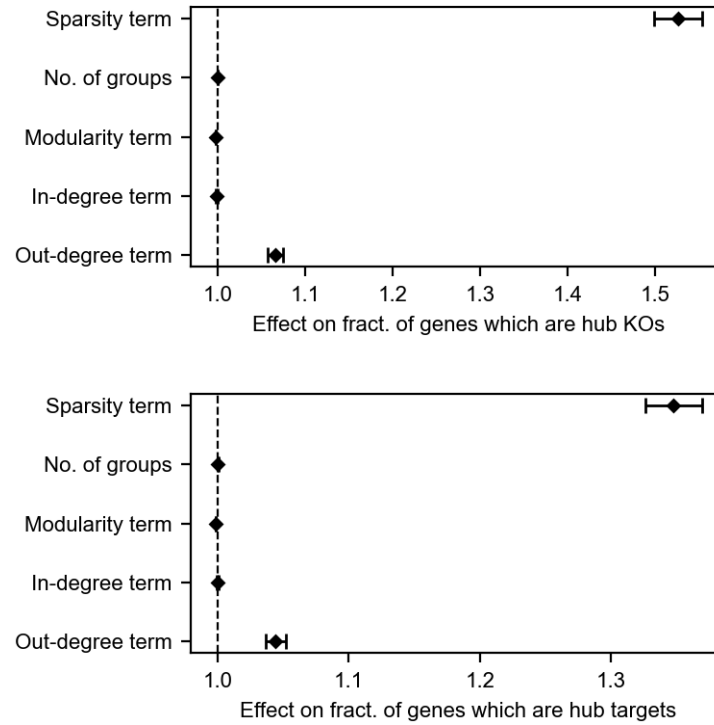


Figure S7: Summary of regression models for effects of network parameters on perturbations. Coefficients from regressing the logit-transformed fraction of genes which are hub knockouts (top) or target genes (bottom) on network generating parameters. Errorbars denote 95% confidence intervals for the regression coefficients. Model summaries can be found in Tables S1 and S2.

Dep. Variable:	logit(pct_ko)	R-squared:	0.587
Model:	OLS	Adj. R-squared:	0.586
Method:	Least Squares	F-statistic:	543.6
Date:	–	Prob (F-statistic):	0.00
Time:	–	Log-Likelihood:	-4167.4
No. Observations:	1920	AIC:	8347.
Df Residuals:	1914	BIC:	8380.
Df Model:	5		
Covariance Type:	nonrobust		

	coef	std err	t	P> t	[0.025	0.975]
const	-6.9629	0.115	-60.458	0.000	-7.189	-6.737
r	0.4229	0.009	46.789	0.000	0.405	0.441
k_adj	0.0004	6.18e-05	6.857	0.000	0.000	0.001
w	-0.0023	0.000	-15.724	0.000	-0.003	-0.002
delta_in	-0.0012	0.000	-2.801	0.005	-0.002	-0.000
delta_out	0.0637	0.004	15.061	0.000	0.055	0.072

Table S1: Summary of regression results (fraction of genes which are hub knockouts).

Dep. Variable:	logit(pct_tg)	R-squared:	0.461
Model:	OLS	Adj. R-squared:	0.460
Method:	Least Squares	F-statistic:	327.7
Date:	–	Prob (F-statistic):	6.30e-254
Time:	–	Log-Likelihood:	-3973.5
No. Observations:	1920	AIC:	7959.
Df Residuals:	1914	BIC:	7992.
Df Model:	5		
Covariance Type:	nonrobust		

	coef	std err	t	P> t	[0.025	0.975]
const	-4.7854	0.104	-45.966	0.000	-4.990	-4.581
r	0.2983	0.008	36.514	0.000	0.282	0.314
k_adj	0.0003	5.59e-05	5.686	0.000	0.000	0.000
w	-0.0016	0.000	-12.002	0.000	-0.002	-0.001
delta_in	-0.0002	0.000	-0.438	0.661	-0.001	0.001
delta_out	0.0433	0.004	11.345	0.000	0.036	0.051

Table S2: Summary of regression results (fraction of genes which are hub target genes).

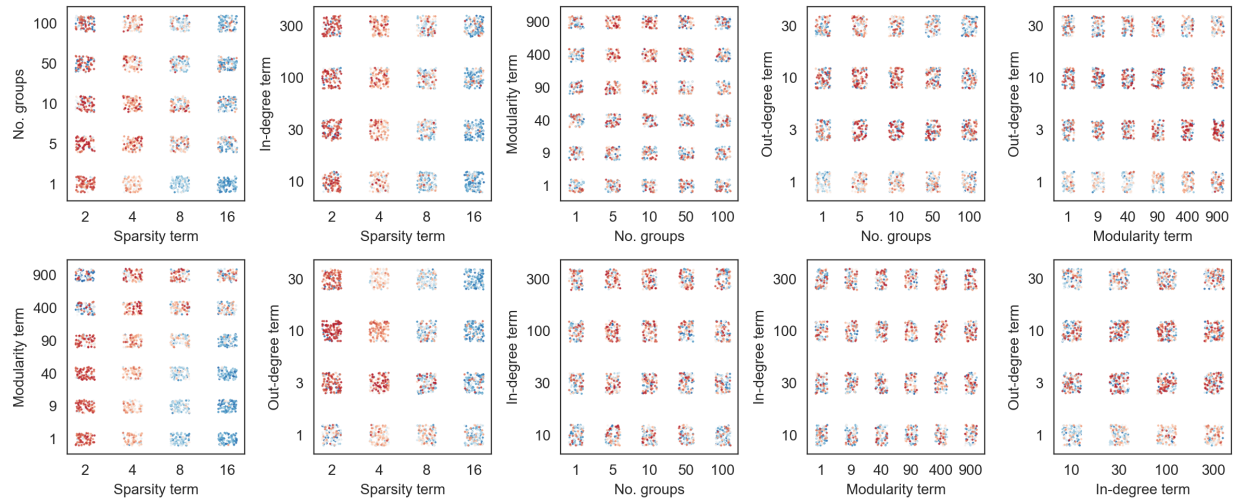


Figure S8: No interaction between network generating parameters and fit to experimental data. As in Fig. 5C-E, we show the relationship between pairs of network generating parameters and goodness of fit to the cumulative distribution of perturbation effects from experimental Perturb-seq data. Each GRN (one point in every subpanel) is colored by its ranked fit to data: the synthetic GRNs are ranked separately by Kolmogorov-Smirnov p -value for incoming and outgoing perturbation effects, then the sum of these two ranks is used to produce an overall ranking. Intense red color indicates better ranked fit to data, and intense blue color indicates a worse ranking.

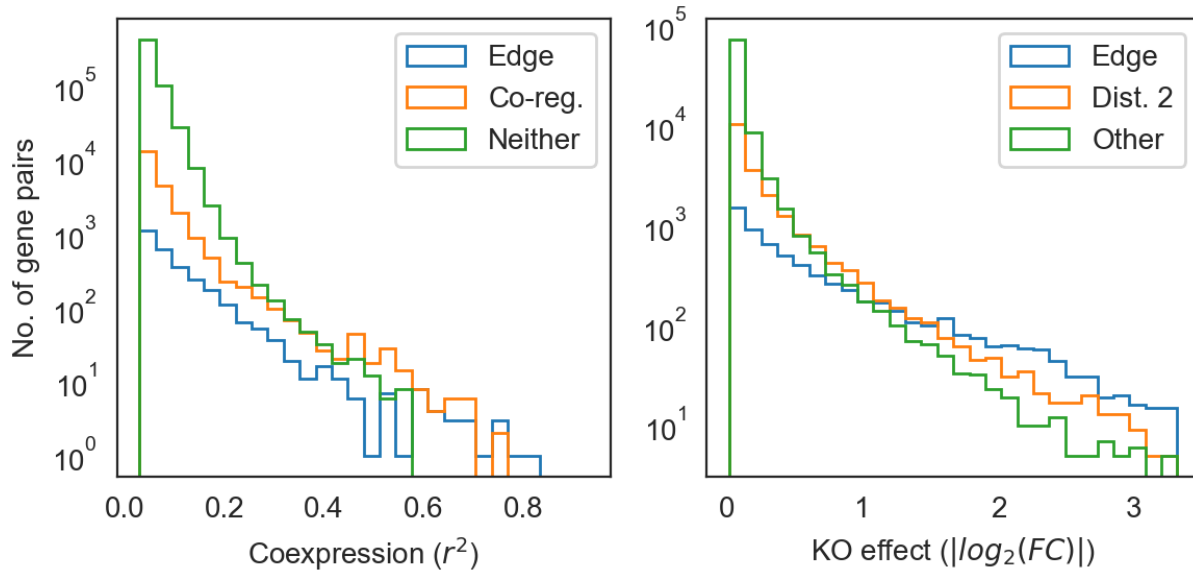


Figure S9: Coexpression is more often due to coregulation than edges. In the focal GRN from Fig. 6, we show a histogram of coexpression values split by whether pairs of genes share an edge (“A regulates B, or B regulates A”, or “A and B are coregulated”), or have another relationship (left panel). Similarly, for perturbation effects, we show the distribution split by whether pairs of genes share an edge (“A regulates B”), a path of distance 2 (“A indirectly regulates B”), or another relationship (right panel). At nearly all levels of coexpression, coregulation is more common than direct regulation. Meanwhile, direct regulation is more common than indirect regulation for the largest perturbation effects – note that the range of KO effects is clipped as in Fig. 6.

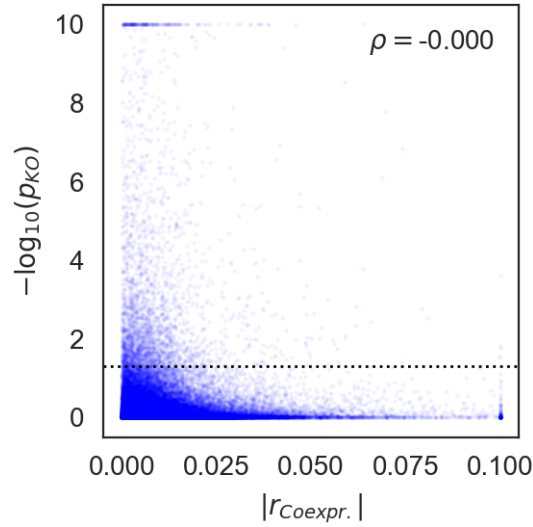


Figure S10: Baseline coexpression and perturbation effects are uncorrelated in Perturb-seq data. Same as **Fig. 6E**, using data from our analysis subset of Replogle *et. al.* 2022 [9]. Gene co-expression (x-axis) is the unsigned Pearson correlation between normalized single-cell gene expression data from unperturbed cells (clipped at $|r| = 0.1$). Perturbation effects (y-axis) are pairwise log-transformed Anderson-Darling p-values for differences in gene expression distribution between perturbed and unperturbed states (clipped at $-\log_{10}(p) = 10$). Rank correlation (Spearman's ρ) is computed on the transformed but not clipped values of these two statistics.

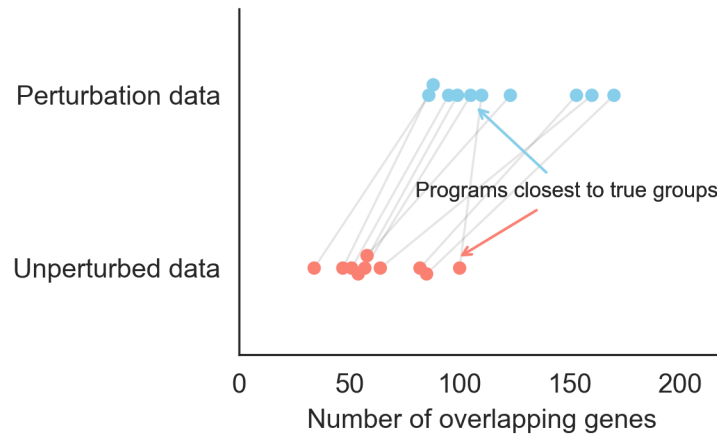


Figure S11: True groups in the synthetic GRN are represented among gene programs. In the focal GRN from Fig. 7, we show the overlap between each of the true groups ($k = 10$, shown as points in each of the bins on the y -axis) and its closest matching program (maximum overlap across all 50 gene sets, values shown on the x -axis). Points corresponding to the same true group are connected with a line spanning across y -axis bins. There is similar representation of all of the groups among the learned gene programs, regardless of input data type.

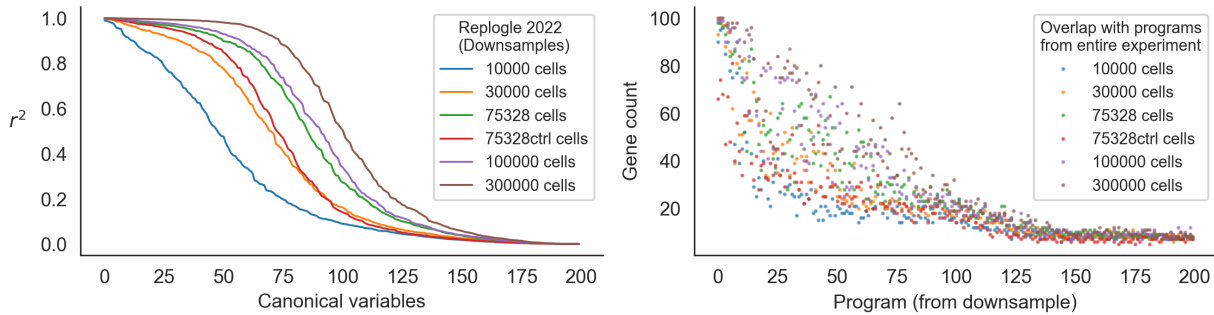


Figure S12: Program replication depends on the number of cells. Same as Fig 7C,D – instead of taking downsamples of unperturbed cells from Replogle *et. al.*, 2022, we here downsample the entire experiment to various study sizes. Here, the “entire experiment” is the normalized expression measurements of 5,247 genes in 932,593 control and intervened-upon cells which received one of the 5,247 perturbations in our analysis subset (**Methods**). We compare singular vectors (left) and programs (right) from the resulting downsamples of the entire experiment, as well as the subsets from Fig 7C,D. We note that the 75,328 control cells replicate the programs from the entire dataset comparably to 30,000 cells from the entire experiment.

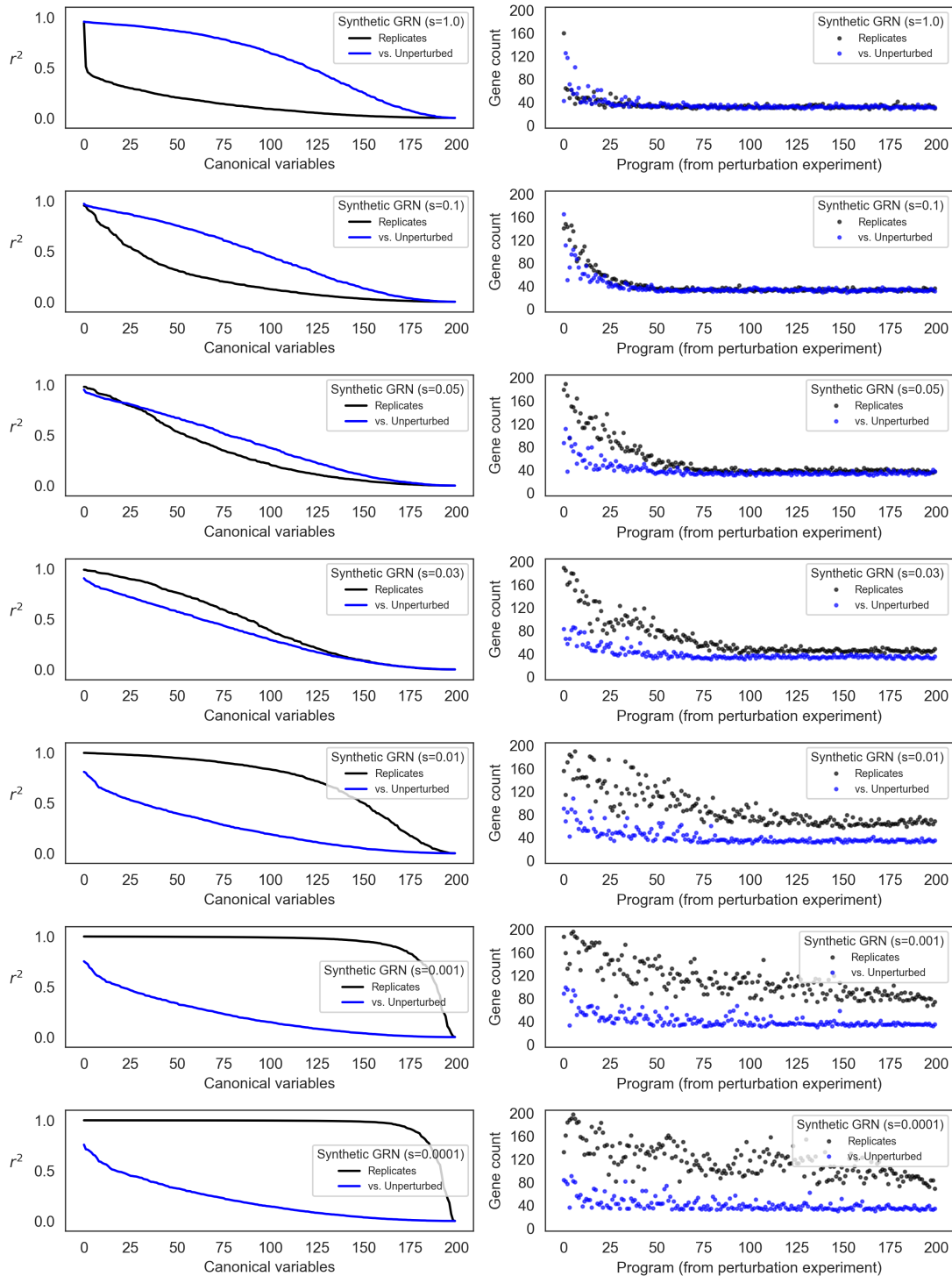


Figure S13: Program replication depends on the magnitude of intrinsic noise. Same as Fig 7A,B for different levels of noise. We repeat CCA and analysis of gene programs as in Fig 7 (see **Methods**), varying the level of intrinsic noise (s). At low levels of noise (small s), replicates from perturbed conditions are much more similar to one another than to the unperturbed data. At high levels of noise (large s), the perturbed data are more similar by canonical correlation to the unperturbed data than to the replicate perturbed data; but programs derived from each of the singular vectors are equivalently reproducible across conditions.